國 立 交 通 大 學

電 子 物 理 研 究 所

碩 士 論 文

介觀系統中電偶極引起的自旋共振

ELECTRIC-DIPOLE-INDUCED SPIN RESONANCE IN MESOSCOPIC SYSTEM

研 究 生：邱志宣

指導教授：朱仲夏教授

中華民國九十七年七月

介觀系統中電偶極引起的自旋共振

研究生：邱志宣　　指導教授：朱仲夏教授

國立交通大學

電子物理研究所

摘要

此論文主要探索在經過Rashba形式量子通道的介觀傳輸系統中由電偶極引起的自旋共振（EDSR）現象。EDSR 的形態包含了沿著通道方向的一個靜態的磁場和一個平行於磁場的交流電場。

用時間微擾產生出的旁帶（sideband）研究了傳輸後波函數的自旋翻轉。在入射能量因微擾而落到黎曼間隙外（旁帶能量為 $\varepsilon \pm \omega$）的情況下，上旁帶和下旁帶包含了 intraband（interbabd）躍遷此無（有）自旋翻轉。

我們主要的發現在自旋翻轉共振特徵存在，當能量吻合黎曼間隙的邊緣或是副帶（sideband）的底端，也就是狀態密度很大的時候。更進一步發現自旋密度在空間有震盪現象是基於由有自旋翻轉和無自旋翻轉的波函數的干涉產生出的。此外，由上下（$\varepsilon \pm \omega$）兩旁帶的自旋密度震盪產生的干涉會有自旋密度拍（beat）。

次之，我們的計算包括 evanescent modes 的效應。我們做了仔細的 evanescent modes 分析，在能量低於副帶底的時候，縱方向波量 k_x 被發現是複數而非存虛數。

Electric-dipole-induced spin resonance in mesoscopic system

Student: Zhi-Hsung Chiu Advisor: Prof. Chon-Saar Chu

Department of Electrophysics

National Chiao Tung University

Abstract

This thesis seeks after the manifestation of the electric-dipole-induced spin resonance (EDSR) in mesoscopics transport through a Rashba-type quantum channel. The EDSR configuration involves a static field along the channel and an ac electric field in parallel with the magnetic field.

Within a time dependent perturbation that induces first sideband, we study the spin flipping in the transmitted wavefunction. For the case when the incident energy falls within the Zeeman gap, and the sideband energies ($\varepsilon \pm \omega$) outside of it, both the upper and lower sideband involves intraband (interband) transition which is nonspin (spin) flipping. Our major finding is that the spin flipping component exhibits resonance characteristics when the sideband energy coincides with either the Zeeman gap edges or the subband bottom, when the density of state is large. Furthermore, the spin density oscillates in space according to the interference between the spin-flipping and non-spin-flipping comments. Additional beating features in the spin density spatial profile is found to result from the interference between the spin density oscillations due to $(\varepsilon + \omega)$ and $(\varepsilon - \omega)$ sidebands.

Our calculation has incorporated the effects of evanescent modes. We have performed a detail analyze on the evanescent modes. The longitudinal wavevector k_x is found to be complex rather then pure imaginary.

致謝

感謝朱老師的指導，清楚的觀念、銳利的想法、無比的耐心，兩年裡替我未來作研究做了最好的示範，讓我獲益良多。並感謝口試委員在颱風天冒雨前來替學生口試，提點學生需要給改進之處，特別感謝許老師逐字訂正論文缺失。也感謝唐志雄學長和王律堯學長給我許多相當有幫助的傳承與意見，使我論文順利完成。還感謝實驗室的好夥伴們學長榮興、冠伊、吉偉，學弟小明、達克、阿杜和 Tihn 在日常生活裡相處愉快時光。最感謝的是爸媽、哥哥的栽培、支持與關懷，使我能全心全力完成學位。感謝交大、電物所有人力、資源給的幫忙。Thanks everyone、Thanks everything、thanks God.

Contents

List of Figures

Chapter 1

Introduction

Manipulation of electron spin by pure electrical method is a challenging target for the scientists. Ever since Dirac proposed, in 1928, his Dirac equation that leads to spin particles and spin-orbit interaction(SOI) in the non-relativistic regime, the utilizationof electron spin for applications has been very limited, due to the small spin-orbit interaction in vacuum. The spin-orbit coupling is such enhanced in narrow gap semiconductors. In the case of bulk inversion asymmetry(BIA), the spin-orbit interaction is the so-call Dresselhaus SOI[1]. A most prominent example is in zinc-blende semiconductors. In case of structure inversion asymmetry(SIA), the SOI is the so-call Rashba SOI[2]. A prominent example is in asymmetric quantum wells. Most recently, it was proposed to invoke the Rashba SOI for the generation of spin resonance without the need of ac magnetic fields.

1.1 Motivation: Electric-dipole-induced spin resonance (EDSR)

The basic physical concepts of EDSR [3][4][5] are analogous to those of nuclear magnetic resonance (NMR). We revisit NMR in Appendix A. The resonance occurs when the frequency of an external rotating magnetic field closely matches the Larmor frequency of spin precession in a static magnetic field. Our fundamental idea of the paper base on

the concept that employ an effective magnetic field due to spin orbital interaction(SOI) instead of the external rotating magnetic field.

In 2006, M.Duckheim and D. Loss [3] point out that one can take advantage of EDSR mechanism to manufacture the out-of-plane magnetization which is robust in the presence of disorder. The system they considered is a semiconductor nanochannel in the diffusive regime and is applied by external fields of a longitudinal a.c. electric field and a parallel static magnetic in-plane.

Accordingly, we can not help ourself to ask the question "What would be the EDSR effects in a mesoscopic system of ballistic quantum channel?" we shall expect a new physics appearance that spin resonance process should involve also inelastic intra-subband transitions. The system we considered is a quantum wells with Rashba spin orbit interaction and is applied externally static in-plane magnetic field along longitudinal direction in the all channel. And a longitudinal a.c. electric field is applied locally on a region of the channel. The a.c. electric field not only drive the electron oscillate but also perform the inelastic scattering to higher or lower energy levels. If the side band energy matches the energy with large density of state and then spin-flip resonance occur. We will give detailed discussions about time modulated wavefunction and one side band approximation in the Chapters 3 and 4.

1.2 Motivation: Energy spectra of Evanescent mode

The processes of transitions to lower subbands bottom or into Zeeman gap should involve Evanescent modes. Because of an external d.c. in-plane magnetic field can not be absent from EDSR. The magnetic field lifts the degeneracy of two spin states which both are zero-momentum states. This give rise to the Zeeman splitting phenomenon and Evanescent modes exist inside the gap.

Very recently, the importance of the evanescent modes has been pointed out by other groups also. L.Serra's group publish "Strongly modulated transmission of a spin-split

quantum wire with local Rashba interaction" [6]. They point out what the role played by Evanescent mode and how does it affect the quantum transport; Z.Q. Yang's group publish "Influence of evanescent waves on spin polarization in a ballistic Rashba bar" [7][8]. They find out the pure evanescent waves can lead to obvious variations of spin polarization near the interfaces up to a range of several hundred nanometers.

Besides,we will discuss another kind of evanescent modes out of the gap which have not been discussed numerously so far. The two kinds of Evanescent modes have different behaviors individually. we will give detailed discussions about energy dispersions and wavefunctions including evanescent modes the Chapters 2 and 4.

Chapter 2

Basic physical structures considered in this work

In this chapter, we will introduce our system profile and its Hamiltonian and wavefunctions without modulated time term, a.c. electric field, in the first section. In the second section, we will use perturbed method to calculate the energy dispersion which involve subband mixing term due to Rashba interaction analytically. And we use numerical method to get an identical result to confirm it. In the following section, in order to obtain all kinds of energy dispersion including evanescent modes, they will be discussed in magnetic fields with different magnitudes.

2.1 Basic Structure of our mesoscopic system

Schematic illustration of the Rashba-type quantum channel based on heterostructure InAs/GaSb is shown in Fig. 2.1. And an in-plane magnetic field $\mathbf{B}$ is applied in the $\hat{\mathbf{x}}$ axis as well as a time-modulated electric field $\mathbf{E}(t)$ is applied parallel with $\mathbf{B}$. Due to structure inversion asymmetry in heterostructure in Fig. 2.2, a build-in electric field is induced and electron moving in 2DEG can be affected by an effective magnetic field, leading to Rashba spin-orbital interaction. The experimental parameter are give by: electron con-

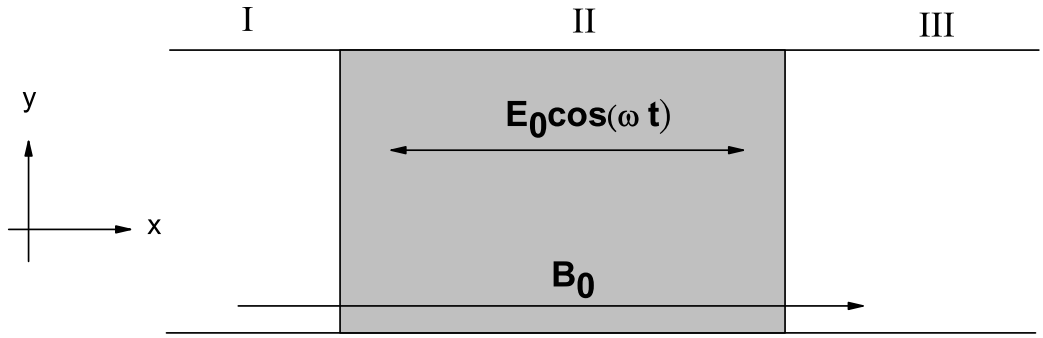

Figure 2.1: Top view of the mesoscopic system. In the all quantum channel, there are Rashba SOI and in-plane d.c. magnetic field along longitudinal direction. And an a.c. electric field is applied locally on gray region.

centration $n_e = 5.7 \times 10^{11}\text{cm}^{-2}$, effective mass $m^* = 0.023\, m_e$, Rashba strength constant $\alpha = 0.94 \times 10^{-11}$(evm) [9], Lande g-factor $g = 8$ [10], width of channel $d = 41.5$(nm); magnetic field strength $\mathbf{B} = 2.656$ (mT). The time-modulated field is $\mathbf{E_0}cos(\omega t)$ with frequency $\omega = 2.058 \times 10^{-1}$ (GHz), electric field strength $\mathbf{E_0} = 5.472 \times 10^{-5}$ (kvolt/cm)

The Hamiltonian of the system can be written as the expression

$$H = \frac{1}{2m}\left[\mathbf{p} + e\mathbf{A}(t)\theta(\frac{L}{2} - |x|)\right]^2 + \left[\Omega\left(\mathbf{p} + e\mathbf{A}(t)\theta(\frac{L}{2} - |x|)\right) + \mathbf{b}_0\right] \cdot \sigma + V_c \quad (2.1)$$

where the spin-orbital field is $\mathbf{\Omega}(p) = \alpha\mathbf{p} \times \hat{e}_z$, $\mathbf{A} = -\int^t dt'\mathbf{E_0}(t') = -\frac{E_0}{\omega}\sin(\omega t)\hat{x}$ is a vector potential corresponding to electric field $\mathbf{E}(t) = E_0\cos(\omega t)\hat{x}$, $\theta(\frac{L}{2} - |x|)$ is a step function, $\mathbf{b}_0 = \frac{g\mu_0}{2}\mathbf{B}_0$ is the energy due to magnetic field along x-direction; V_c is a confining potential in y-direction; $V_c = 0$ for $y = 0 \sim d$ and $V_c = \infty$ otherwise.

In order to simplify our calculation loading, the dimensionless Hamiltonian is introduced by choosing proper physical units. Length a is in the unit of Fermi wavelength,$a^* = \lambda_f = 5.28nm$; energy E in the unit of Fermi energy $E^* = \frac{\hbar^2 k_f^2}{2m^*} = 59.5mev$, frequency ω in the unit of $\omega^* = \frac{E^*}{\hbar}$, time t in the unit $t^* = \frac{\hbar}{E^*}$, electric field strength E_0 in the unit of $E_0^* = \frac{E^*}{ea^*}$, Rashba constant α in the unit of $\alpha^* = \frac{E^*}{\hbar k_f}$. After standard dimensionless

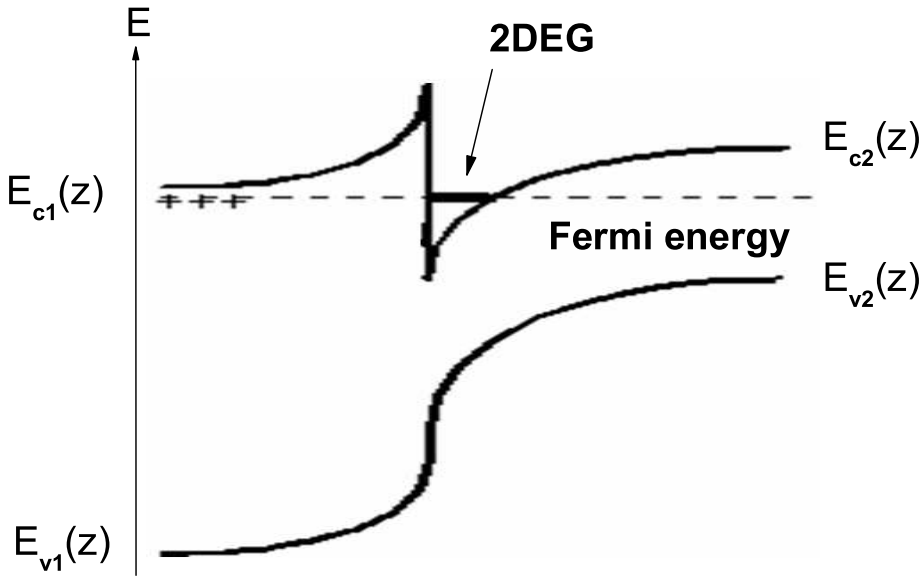

Figure 2.2: Sketch of heterostructures potential profile. E_{c1} is conduction band energy of material 1, InAs; E_{v1} is valence band energy of material 1, InAs; Material 2 is GaSb. Electric field is form InAs toward GaSb.

process, one obtain

$$H(x,y,t) = \\ -\left[\frac{\partial}{\partial x} - i\frac{E_0}{\omega}\sin(\omega t)\theta\left(\frac{L}{2}-|x|\right)\right]^2 + \frac{\alpha}{i}\left(-\frac{\partial}{\partial x}\sigma_y + \frac{\partial}{\partial y}\sigma_x\right) + \frac{\alpha E_0 \sin(\omega t)}{\omega}\theta\left(\frac{L}{2}-|x|\right)\sigma_y \\ +b_0\cdot\sigma_x - \frac{\partial^2}{\partial y^2} + V_c \tag{2.2}$$

The first of overall, the influence of a.c. electric field is not considered in this chapter, we turn off electric field, $E_0 = 0$, to find wavefunctions and energy spectra.

$$H(x,y) = -\frac{\partial^2}{\partial x^2} - \frac{\partial^2}{\partial y^2} - \alpha\frac{1}{i}\frac{\partial}{\partial x}\sigma_y + \alpha\frac{1}{i}\frac{\partial}{\partial y}\sigma_x + b_0\sigma_x + V_c(y) \tag{2.3}$$

2.2 Electronic states

In this section, we will discuss two modes of electron energy spectrum. First part, for propagating mode, the perturbed method can be employed to get the energy dispersion analytically. Besides, we can also numerically obtain very well-agreed result to compare with perturbed result. In the second part for evanescent mode, we use secular equation and quadratic solution to solve the evanescent momenta k for a given E which point out electron energy spectrum of evanescent mode.

2.2.1 Insignificant effect in Rashba-induced subband mixing

In this subsection, we analytically solve wavefunction and electron energy spectrum for the Hamiltonian Eq. (2.3) without dropping the Rashba-induced subband mixing term $\frac{\alpha}{i}\frac{\partial}{\partial y}\sigma_x$ with the perturbed method. Then, we use numerical method to get electron energy spectrum to confirm the previous result. First, we treat $\frac{\alpha}{i}\frac{\partial}{\partial y}\sigma_x$ term as perturbed term and have to drop it to get the exact wavefunction as the basis for complete wavefunction including an influence of subband mixing. Accordingly we employ the time independent Schrodinger equation

$$H_0\Psi_{n\sigma} = E^{(0)}_{n\sigma}\Psi_{n\sigma} \tag{2.4}$$

where n denotes subband index due to energy splitting from confining potential in y axis, σ denote for different branches in the same subband.

$$H_0 = -\frac{\partial^2}{\partial x^2} - \frac{\partial^2}{\partial y^2} - \alpha\frac{1}{i}\frac{\partial}{\partial x}\sigma_y + b_0\sigma_x + V_c(y) \tag{2.5}$$

and $\Psi_{n\sigma}$ can be expanded by spatial wavefunction and spin state, $\psi(x)\phi_n(y)\chi_\sigma$. Since electron in x-direction is free without any scatterer, the momentum $\mathbf{k}$ is a good quantum

number to label the state, we can easily obtain plane-wave wavefunction along x-direction

$$\psi(x) = e^{ikx} \tag{2.6}$$

Because we choose a hard wall confinement in the lateral direction, the well-known solution

$$\phi_n(y) = \sqrt{\frac{\pi}{d}} \sin\left(\frac{n\pi}{d}y\right) \text{ and } \varepsilon_{\mathrm{n}}^{(0)} = \left(\frac{n\pi}{d}\right)^2 \tag{2.7}$$

can be found in any Quantum mechanics text book. Last one unknown spin state, χ_σ, can be obtained by solving eigenvalue problem for eigenstate and eigenenergy

$$\chi_\sigma = \frac{1}{\sqrt{2}} \begin{pmatrix} -\sigma \frac{i\alpha k + b_0}{\sqrt{b_0^2 + \alpha^2 k^2}} \\ 1 \end{pmatrix} \tag{2.8}$$

$$E_{n\sigma}^{(0)} = k^2 + \varepsilon_{\mathrm{n}}^{(0)} - \sigma\sqrt{b_0^2 + \alpha^2 k^2},\ \sigma = \pm 1 \tag{2.9}$$

where n is the subband index due to the energy splitting of lateral confinement potential; the σ is the index of branches in the same subband. See Fig. 2.3

After we have prepared those basis already, the Hamiltonian including the perturbed term $\frac{\alpha}{i}\frac{\partial}{\partial y}\sigma_x$ becomes

$$H = H_0 + H' = \left(k^2 - \frac{\partial^2}{\partial y^2} - \alpha k \frac{\partial}{\partial x}\sigma_y + b_0\sigma_x + V_c(y)\right) + \left(\alpha \frac{1}{i}\frac{\partial}{\partial y}\sigma_x\right) \tag{2.10}$$

And perturbed wavefunction is represented as

$$\psi_{n\sigma}(y) = \phi_n(y)\chi_\sigma + \sum_{n'\neq n, \sigma'\neq\sigma} c_{n'\sigma'}\phi_{n'}(y)\chi_{\sigma'} + \sum_{n''\neq n, \sigma''\neq\sigma} c_{n''\sigma''}\phi_{n''}(y)\chi_{\sigma''} + \ldots \tag{2.11}$$

where $c_{n'\sigma'}$ is the first order correction coefficient; $c_{n''\sigma''}$ is the second order correction coefficient and so on.

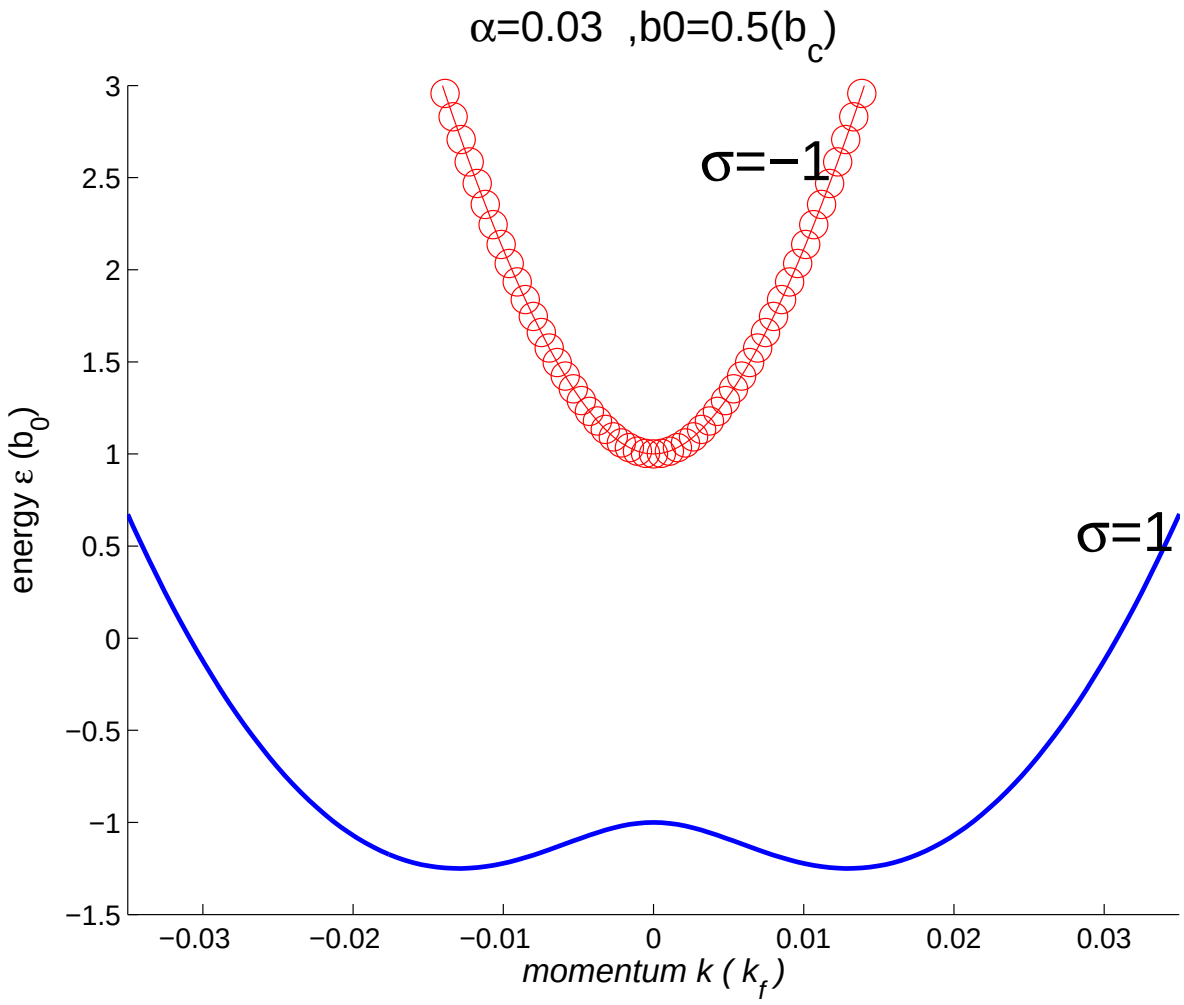

Figure 2.3: Two branches in the same subband, the first subband n=1. The $\sigma = 1$ branch is plotted by blue line; The other branch $\sigma = -1$ is plotted by red line with empty dot.x-axis is momentum k in unit of $k_f = 1.89 \times 10^8 (1/m)$; y-axis is energy E in unit of $b_0 = 0.013(mev)$.

After detailed calculation process, the result of first order correlation to energy $E^{(1)}_{n\sigma} = 0$ and correction coefficient to wavefunction is shown

$$c^{(1)}_{m\sigma'} = \frac{\frac{\alpha}{i}\left(\frac{2}{d}n\Delta_{mn}\right)\left(\chi^{\dagger}_{\sigma'}\sigma_x\chi_{\sigma}\right)}{\left(E^{(0)}_{n\sigma} - E^{(0)}_{m\sigma'}\right)},\ m \neq n \tag{2.12}$$

We can go on calculating the second order correction to energy and show

$$E^{(2)}_{n\sigma} = \sum_{n'\neq n,\sigma\neq\sigma'} c^{(1)}_{n'\sigma'}\left(\frac{\alpha}{i}\frac{2}{d}n'\Delta_{nn'}\right)\chi^{\dagger}_{\sigma}\sigma_x\chi_{\sigma'} \tag{2.13}$$

where $c^{(1)}$ is first order correction coefficients to wavefunction; $\Delta_{nn'}$ is coupling factor between two different subband.

$$\Delta_{nn'} = \left[1 - (-1)^{n-n'}\right]\left[\frac{n}{(n^2 - n'^2)}\right] \tag{2.14}$$

In Eq. (2.13), we sum enough n' and the result turns out $E^{(2)}_{n\sigma} = -0.25\alpha^2$. Typically max of $n' = 100$ can give a good convergence.

Here we have to mention a brief summary for the result of perturbed method that the correction of Rashba-induced subband mixing to energy is an insignificant effect. The effect is a second order correction.

In order to confirm previous result we use numerical method to calculate energy dispersion again. And the assuming Schrödinger equation [7][8] generally be expressed by

$$\left[k^2 + \left(\frac{m\pi}{d}\right)^2 - \alpha_1 k\sigma_y + b_0\sigma_x\right]\begin{bmatrix} C_m(k) \\ D_m(k) \end{bmatrix} + \frac{2}{\pi}\sum_{n\neq m}\left[\frac{\alpha_2}{i}\frac{n\pi}{d}\sigma_x\right]\Delta_{mn}\begin{bmatrix} C_n(k) \\ D_n(k) \end{bmatrix} = E_{(k)}\begin{bmatrix} C_m(k) \\ D_m(k) \end{bmatrix} \tag{2.15}$$

where $[C_m(k)\ D_m(k)]^T$ is an assuming wavefunction.

Eq. (2.15) can be reduced to the compact matrix form is shown following.

$$\begin{cases} \left(k^2+\left(\frac{m\pi}{d}\right)^2-E_{(k)}\right)C_m(k)+\sum_n\left(\frac{\alpha}{i}\frac{n\pi}{d}\frac{2}{\pi}\Delta_{mn}+i\alpha k\delta_{nm}+b_0\delta_{nm}\right)D_n(k)=0 \\ \left(k^2+\left(\frac{m\pi}{d}\right)^2-E_{(k)}\right)D_m(k)+\sum_n\left(\frac{\alpha}{i}\frac{n\pi}{d}\frac{2}{\pi}\Delta_{mn}-i\alpha k\delta_{nm}+b_0\delta_{nm}\right)C_n(k)=0 \end{cases} \tag{2.16}$$

The size of matrix is dependent on the number of subbands we considered. For example, if total N=10 (N is maximum of indexes , m and n.) subbands are involved and then the size of matrix is 20×20. Here we can solve 2N eigenenergys for a given k. However we can solve 4N momenta for a given incident energy also.

The numerical result of energy dispersion of the first subband is shown in Fig. 2.4. The correction of subband mixing due to $\frac{\alpha}{i}\frac{\partial}{\partial y}\sigma_x$ is second order and the numerical result is identified with the perturbed result.

2.2.2 Energy spectra of Evanescent mode

In previous part, we know the Rashba-induce subband mixing is so weak that we ignore it and discuss Evanescent modes.

The evanescent modes are [11] found that their behaviors are quite different in weak ($B<B_c$) and strong magnetic field ($B>B_c$). The critical field B_c is given by the Rashba spin-orbit interaction (typically B_c ∼10mT).

We will discuss in three cases: The external magnetic energy is smaller, lager, and equal to the SOI energy due to Rashba effect. The three kinds of evanescent modes have different energy spectra individually.

If Eq. (2.3) does not include $\frac{\alpha}{i}\frac{\partial}{\partial y}\sigma_x$, the Rashba-induced subband mixing term, then each subband labelled by different n is independently described by Hamiltonian H_{0n} and energy Eq. (2.9)

$$H_{0n}=-\frac{\partial^2}{\partial x^2}-\alpha\frac{1}{i}\frac{\partial}{\partial x}\sigma_y+b_0\sigma_x+\varepsilon_n \tag{2.17}$$

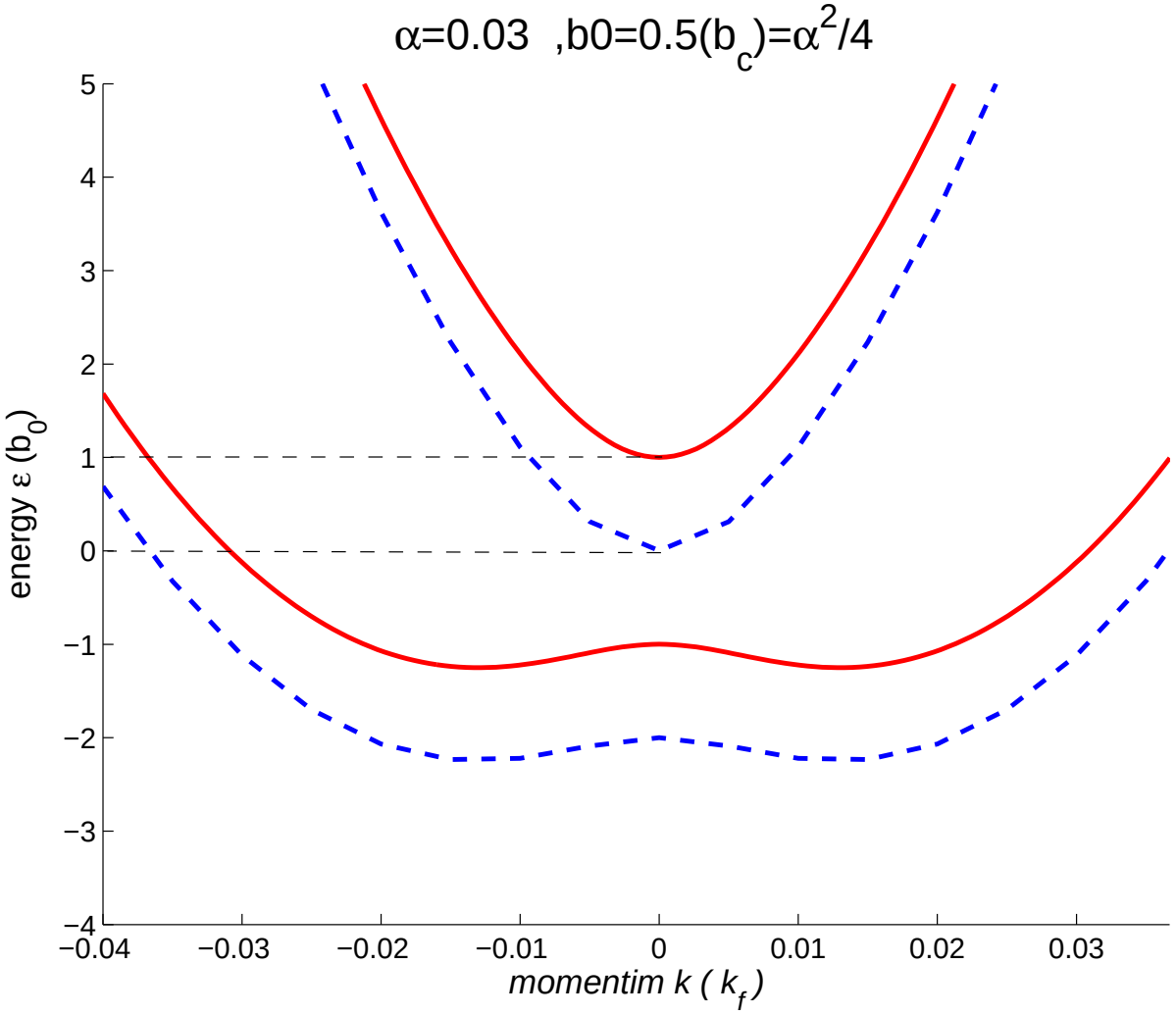

Figure 2.4: Comparing energy in the first subband with and without perturbed term $\frac{\alpha}{i}\frac{\partial}{\partial y}\sigma_x$. The unperturbed energy is plotted by red solid line and perturbed energy is plotted by blue dashed line. They are a difference of $\alpha^2/4 = 2.5 \times 10^{-4}$. The numerical result of correction to energy dispersion due to subband mixing term is identified with the perturbed result. X-axis is momentum k in unit of $k_f = 1.89 \times 10^8(1/m)$; y-axis is energy E in unit of $b_0 = 0.013(mev)$.

The two energy spectra of Zeeman and Rashba regimes have one different character at zero momentum **k**. The second derivative is positive(negtive) in former(latter) regime. The character gives us a good criterion to determinate the magnitude of the critical magnetic field b_c. We can take derivative on energy dispersion Eq. (2.9) twice and set it zero and the magnitude of critical magnetic energy $b_c = \alpha^2/2$.

We take an example of three magnitudes of magnetic energy, $b_0 < b_c$, $b_0 = b_c$ and $b_0 > b_c$ cases.

For a given energy in arbitrary regime, the four momenta **k** can be obtained analytically by Eq. (2.9) with quadratic relation. The four momenta have different modes in different energy regimes, generally speaking:

1. Above Zeeman gap ($E - \varepsilon_1 > b_0$): Four momenta in two branches are all real, propagating modes.

2. Between Zeeman gap ($b_0 > E - \varepsilon_1 > -b_0$): Two momenta **k** in outside branch, $\sigma = 1$, are real and two momenta **k** in inside branch, $\sigma = -1$, are pure imaginary, pure evanescent modes.

3. Between subband bottom and low terminal of Zeeman gap [$-b_0 > E - \varepsilon_1 > (\alpha^2/4 - b_0^2/\alpha^2)$], four momenta in two branches are all real, propagating modes.

4. Under subband bottom: Four momenta in two branches are all complex, propagating and evanescent modes couple together.

In $b_0 < b_c$ case, see Fig. 2.5, the magnetic energy is not large enough to compete SOI. Therefore not only the "Rashba" shape is still observable but also the degeneracy at zero **k** is left. In the Zeeman gap, the evanescent mode with pure imaginary momentum **k** which is plotted by blue circle line. Below the subband bottom the other kind of evanescent mode exists that momentum **k** is a complex number, i.e. the evanescent property couple with the propagating property. The real part of this evanescent momentum is almost constant with decreasing energy. And it is worth to mention that the energy of maximum imaginary k in Zeeman gap is $E = \varepsilon_1 - \frac{b_0^2}{\alpha^2}$, i.e the shape of the evanescent mode is not symmetric with respect to the center, $E = \varepsilon_1$.

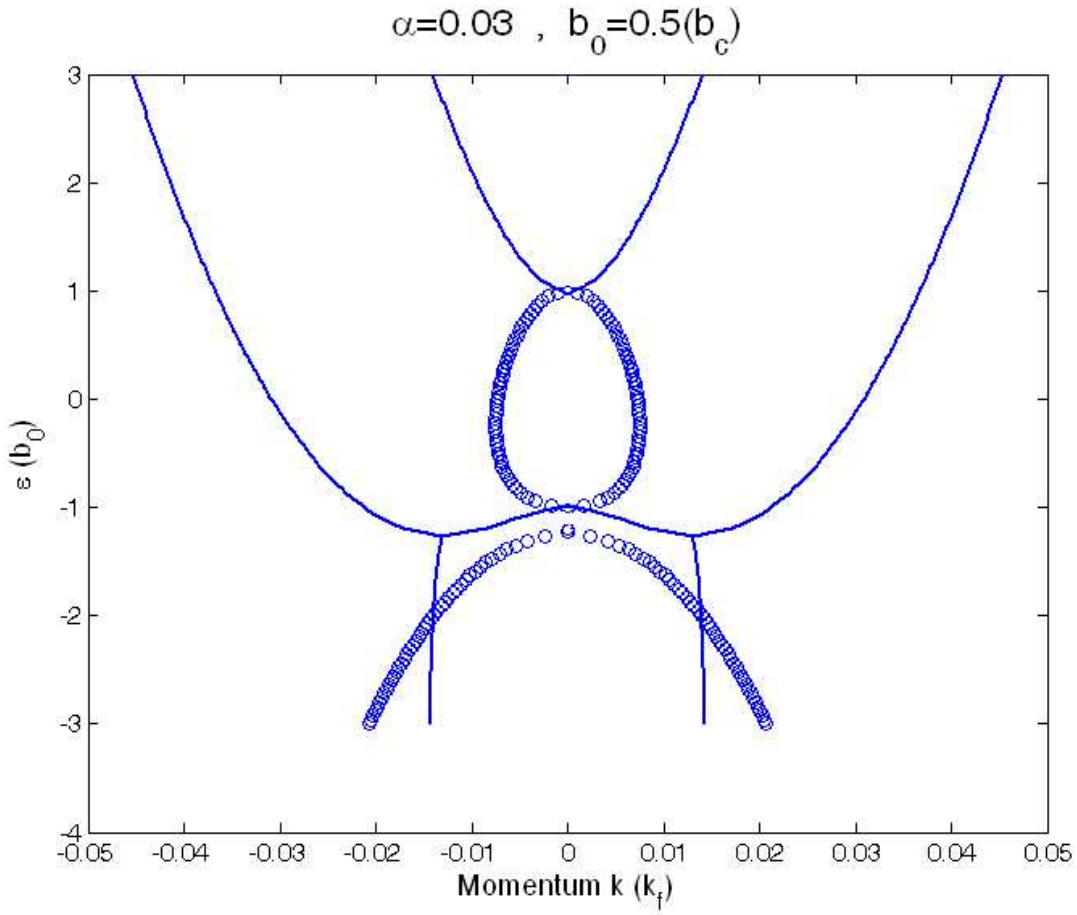

Figure 2.5: Energy dispersion of evanescent mode in magnetic energy small then the SOI energy case.The Rashba effect still dominates. Solided line is propagating mode(k is real). Line with circle is evanescent mode(k is imaginary); Under energy bottom region, the two modes couple together(k is complex). X-axis is momentum k in unit of $k_f = 1.89 \times 10^8 (1/m)$; y-axis is energy E in unit of $b_0 = 0.013(mev)$.

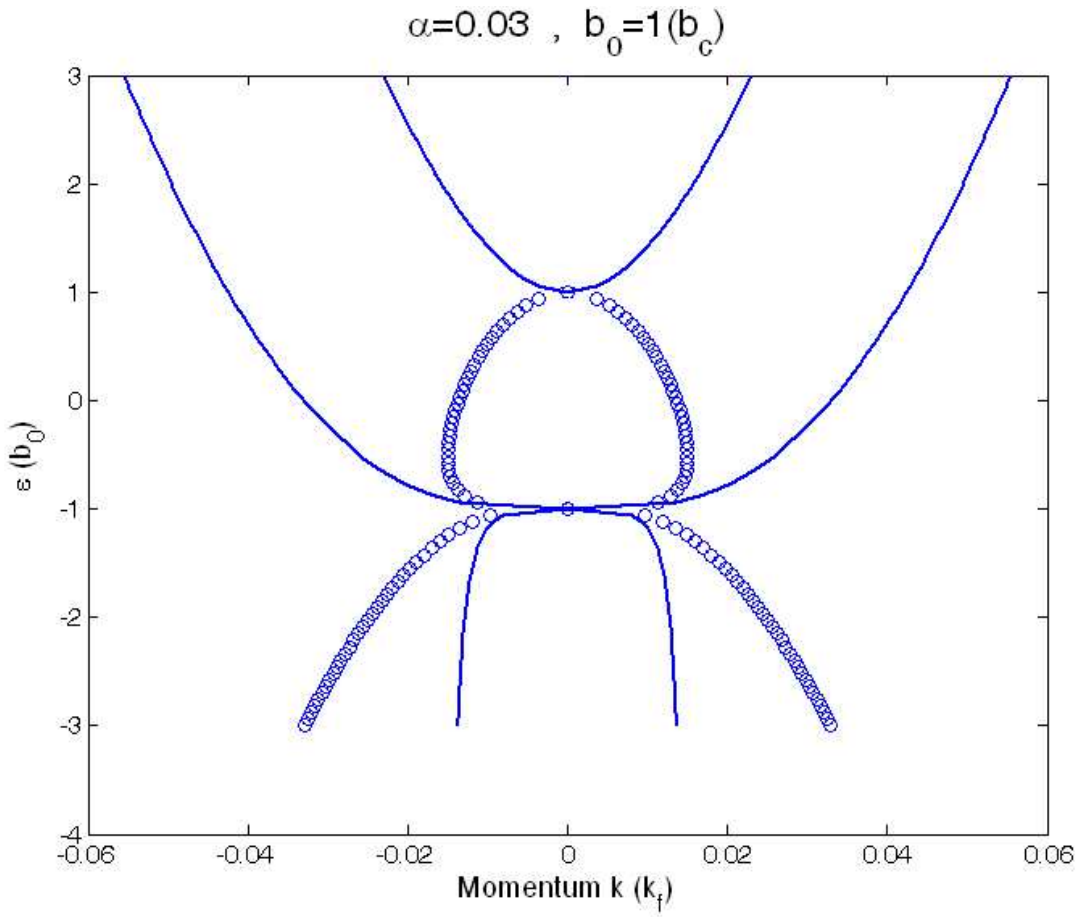

Figure 2.6: Energy dispersion of evanescent mode in magnetic energy equal to the SOI energy case.The Rashba effect and Zeeman effect compete; the subband bottom is flat. Solided line is propagating mode(k is real). Line with circle is evanescent mode(k is imaginary); Under energy bottom region, the tow modes couple together(k is complex). X-axis is momentum k in unit of $k_f = 1.89 \times 10^8(1/m)$; y-axis is energy E in unit of $b_0 = 0.013(mev)$.

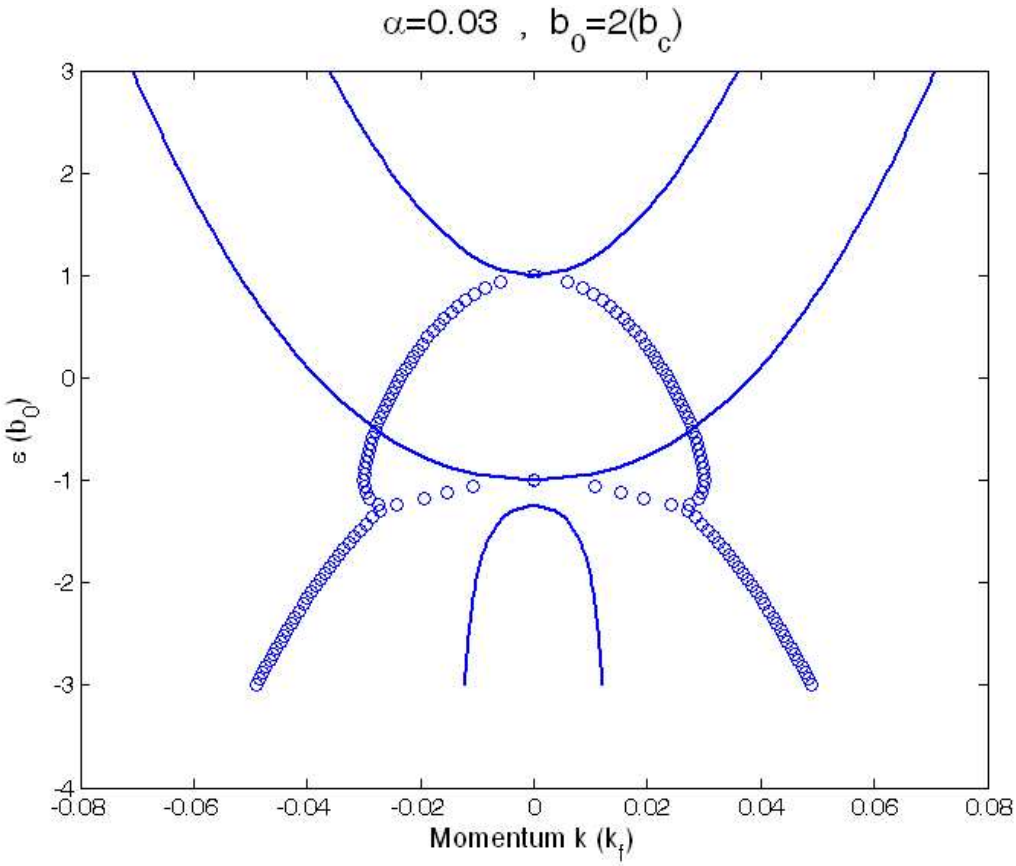

Figure 2.7: Energy dispersion of evanescent mode in magnetic energy larger then the SOI energy case.The Zeeman effect dominates. Solided line is propagating mode(k is real). Line with circle is evanescent mode(k is imaginary); In $E < \varepsilon_1 - \frac{b_0^2}{\alpha^2}$ regime, the two modes couple together(k is complex). X-axis is momentum k in unit of $k_f = 1.89 \times 10^8 (1/m)$; y-axis is energy E in unit of $b_0 = 0.013(mev)$.

In $b_0 = b_c$ case, see Fig. 2.6, the magnetic energy is comparable with the SOI. The feature of Rashba dispersion disappears and the flat subband bottom is a remarkable feature. With increasing magnetic field strength, the $E = \varepsilon_1 - \frac{b_0^2}{\alpha^2}$ is decreasing.

In $b_0 > b_c$ case, see Fig. 2.7, the magnetic energy is larger than the SOI, i.e. Zeeman effect dominates and two parabola dispersions show. Finally, the magnetic field is such large that the energy of maximum imaginary k overstretch the subband bottom. The propagating mode and evanescent mode couple together while the energy lower than $\varepsilon_1 - \frac{b_0^2}{\alpha^2}$.

Chapter 3

Calculation of time modulated wavefunction

In this chapter main work in the first section is to consider about the influence of the time modulated electric field on the wave functions. The influence includes inelastic scattering process and make sidebands attached to wavefunction. In the second section, the number current density is introduced and the interesting thing is the contribution from the interference of intraband wavefunction will be introduced.

3.1 Time modulated wavefunction and transformations

We start to apply the a.c. electric field on our mesoscopic system, Fig. 2.1 mentioned in chapter 2, and calculate the wavefunction.

The time dependent Schrödinger equation is written as

$$H\Psi(\mathbf{r},t) = i\frac{\partial}{\partial t}\Psi(\mathbf{r},t) \tag{3.1}$$

where

$$H = \left[\begin{array}{l} \left(-\dfrac{\partial^2}{\partial x^2} + \dfrac{E_0^2}{\omega^2}\sin^2(wt) + i\dfrac{2E_0}{\omega}\sin(\omega t)\dfrac{\partial}{\partial x} \right) \\ + \left(-\dfrac{\partial^2}{\partial y^2} - \dfrac{\alpha}{i}\dfrac{\partial}{\partial x}\sigma_y + \dfrac{\alpha}{i}\dfrac{\partial}{\partial y}\sigma_x + b_0\sigma_x + V_c + \dfrac{\alpha E_0}{\omega}\sin(\omega t)\sigma_y \right) \end{array} \right] \tag{3.2}$$

But Eq. (3.2) is really too complaint to solve out wavefunction immediately. Here we must employ transformations[12][13] to simplify the "terrible" time-dependent Schrödinger equation.

First we can employ the first transformation

$$\Psi(\mathbf{r}, t) = \exp\left(\frac{iE_0^2 \sin(2\omega t)}{4\omega^3} \right) \psi(\mathbf{r}, t) \tag{3.3}$$

and the identity $2\sin^2(\omega t) = 1 - \cos(2\omega t)$. Substituting transformation Eq. (3.3) into the time dependent Schrödinger equation Eq. (3.1), we have the time dependent Schrödinger equation whose $\frac{E_0^2}{\omega^2}\sin^2(\omega t)$ is eliminated

$$\left[\begin{array}{l} \left(-\dfrac{\partial^2}{\partial x^2} + \dfrac{E_0^2}{2\omega^2} + i\dfrac{2E_0}{\omega}\sin(\omega t)\dfrac{\partial}{\partial x} \right) \\ + \left(-\dfrac{\partial^2}{\partial y^2} - \dfrac{\alpha}{i}\dfrac{\partial}{\partial x}\sigma_y + \dfrac{\alpha}{i}\dfrac{\partial}{\partial y}\sigma_x + b_0\sigma_x + V_c + \dfrac{\alpha E_0}{w}\sin(\omega t)\sigma_y \right) \end{array} \right] \psi(\mathbf{r}, t) = i\frac{\partial}{\partial t}\psi(\mathbf{r}, t) \tag{3.4}$$

Second we use the second transformation.

$$\psi(\mathbf{r}, t) = \exp\left[-\frac{2E_0}{\omega^2}\cos(\omega t)\frac{\partial}{\partial x} \right] f(\mathbf{r}, t) \tag{3.5}$$

Substituting transformation Eq. (3.5) into the time dependent Schrödinger equation Eq. (3.4), we have the time dependent Schrödinger equation whose $i\frac{2E_0}{\omega}\sin(\omega t)\frac{\partial}{\partial x}$ is eliminated

$$\left[\left(-\frac{\partial^2}{\partial x^2}+\frac{E_0^2}{2\omega^2}\right)+\left(-\frac{\partial^2}{\partial y^2}-\frac{\alpha}{i}\frac{\partial}{\partial x}\sigma_y+\frac{\alpha}{i}\frac{\partial}{\partial y}\sigma_x+b_0\sigma_x+V_c+\frac{\alpha E_0}{\omega}\sin(\omega t)\sigma_y\right)\right]f(\mathbf{r},t)$$
$$=i\frac{\partial}{\partial t}f(\mathbf{r},t) \tag{3.6}$$

The first two transformations can eliminate the time dependent terms which do not couple with spin operator σ_y.

Finally we can easily eliminate the constant term with the transformation

$$f(\mathbf{r},t)=\exp\left(-i\frac{E_0^2}{2\omega^2}t\right)g(\mathbf{r},t) \tag{3.7}$$

and get more "simple" time dependent Schrödinger equation

$$\left(-\frac{\partial^2}{\partial x^2}-\frac{\partial^2}{\partial y^2}-\frac{\alpha}{i}\frac{\partial}{\partial x}\sigma_y+\frac{\alpha}{i}\frac{\partial}{\partial y}\sigma_x+b_0\sigma_x+V_c+\frac{\alpha E_0}{w}\sin(\omega t)\sigma_y\right)g(\mathbf{r},t)=i\frac{\partial}{\partial t}g(\mathbf{r},t) \tag{3.8}$$

When an incident wave go into the time dependent region from left infinite, see in Fig. 3.1, the $\frac{\alpha E_0}{\omega}\sin(\omega t)\sigma_y$ term not only gives rise to inelastic scattering precess which change the energy $E\pm\omega$ and momentum $k(E\pm\omega)$ but also produces time modulated wavefunctions which remain the same momentum k with incident wave but their energy change $\pm\omega$.

As is mentioned in previous Chapter 2, plane wave $\psi(x)=e^{ikx}$ and standing wave $\phi_n(y)=\sqrt{\frac{\pi}{d}}\sin\left(\frac{n\pi}{d}y\right)$ are spatial wavefunctions in x and y direction. Substituting them into Eq. (3.8), the wavefunctions of Eq. (3.1) is solved out as fallowing

$$\Psi(\mathbf{r},E,t)=\exp\left(\frac{iE_0^2\sin(2\omega t)}{4\omega^3}\right)\exp\left(-\frac{2E_0}{\omega^2}\cos(\omega t)\frac{\partial}{\partial x}\right)\exp\left(-i\frac{E_0^2}{2\omega^2}t\right)\left[e^{ik(E)x}\phi_n(y)\chi e^{-iEt}\right] \tag{3.9}$$

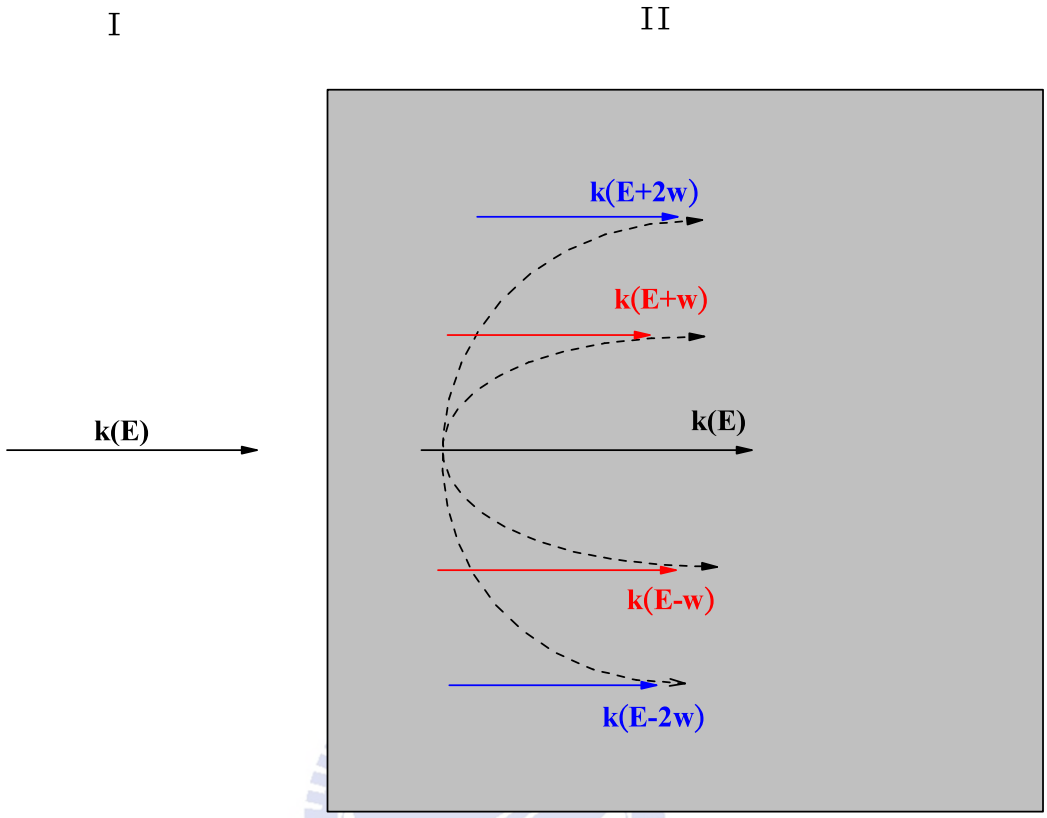

Figure 3.1: Sketch of side band wavefunction due to inelastic scattering process (red and blue solid lines)and time modulated wavefunction (black dotted line) at the first interface between time-independent and time dependent regions. In this figure, the inelastic scattering wavefunctions still have time modulated wavefunctions but are not shown. The unit of frequency ω is in energy unit.

where spin state χ have not determinated. We will determinate it in different energy regimes and explicitly show it in the next chapter.

3.2 Particle current density

In this section we reproduce the current density from the continuity equation. It is worth to mention the contributions to current due to the interference two wavefunctions of the intraband seem to appear and are position-dependent. Here we emphasize that the result

will be demonstrated in detail again in section 4.1.4.

$$\frac{\partial}{\partial t}\rho(\mathbf{r},t) = -\frac{\partial}{\partial x}J(\mathbf{r},t) \tag{3.10}$$

where ρ is number density and J is a particle current density. After performing detailed calculation process for current density in Appendix B, we have the current density expression.

$$J(x,t) = \Psi^{\dagger}(x,t)\left(-i\frac{\partial}{\partial x} - \frac{\alpha}{2}\sigma_y\right)\Psi(x,t) + c.c. \tag{3.11}$$

where Ψ is two components wavefunction and the abbreviation, c.c., is standing for complex conjugate of the former terms. In order to get a steady current result, time average expression is introduced

$$J(x) = \frac{\int_0^T J(x,t)dt}{T} \tag{3.12}$$

where $T = \frac{2\pi}{\omega}$, a periodic duration. And it always is valid when the time scale of the measurement is much greater than the time scale of periodic duration. For an example, we calculate current flow with wavefunction in right time-independent region

$$\begin{aligned}
&\Psi(x,t) = \\
&t_{0\sigma}\exp\left[ik_{R\sigma}x\right]\tilde{\chi}_{R\sigma}e^{-iEt} + t_{0,\bar{\sigma}}\exp\left[ik_{R\bar{\sigma}}x\right]\tilde{\chi}_{R\bar{\sigma}}(E)e^{-iEt} \\
&+t_{1\sigma}\exp\left[ik_{R\sigma+}x\right]\chi_{R\sigma+}e^{-i(E+\omega)t} + t_{1,\bar{\sigma}}\exp\left[ik_{R\bar{\sigma}+}x\right]\chi_{R\bar{\sigma}+}e^{-i(E+\omega)t} \\
&+t_{-1\sigma}\exp\left[ik_{R\sigma-}x\right]\chi_{R\sigma-}e^{-i(E-\omega)t} + t_{-1,\bar{\sigma}}\exp\left[ik_{R\bar{\sigma}-}x\right]\chi_{R\bar{\sigma}-}e^{-i(E-\omega)t}
\end{aligned} \tag{3.13}$$

and it originates from the incident wavefunction $\exp\left[ik_{R\sigma}x\right]\tilde{\chi}_{R\sigma}e^{-iEt}$ with momentum $k_{R\sigma}$ in left time-independent region. Where the first footnote of coefficient denotes the times of electric inelastic scatterer and the $\pm$ for energy absorb or emit a photon; the second footnote denotes branch. And the first footnote of momentum denotes R-ight or L-eft

going, the second one is for branch and third one is for energy absorb or emit a photon.

The transmission involves the effect of the second interface i.e. we have considered the multiple scattering processes. The reason will be explained and calculation will be shown in chapter 4.

Substituting wavefunction Eq. (3.13) into steady current Eq. (3.12), we can get a steady current expression. Because the different energy domains, E and $E\pm\omega$, are orthogonal in one periodic duration. However the current density expression looks like position-dependent which mean the electron accumulation or disappearance occurs. Besides, it is very not conventional terms, the crossing terms due to the two the non-orthogonal spin state χ.

$$
\begin{aligned}
&\frac{1}{T}\int_0^T J(x,t)dt = \\
&\left(\begin{array}{l}
\exp\left[-i\left(k^*_{R\sigma}-k_{R\sigma}\right)x\right]\left[\left(k^*_{R\sigma}+k_{R\sigma}\right)-\alpha\tilde{\chi}^+_{R\sigma}\sigma_y\tilde{\chi}_{R\sigma}\right] \\
+\left(t^*_{1\sigma}t_{1\sigma}\right)\exp\left[-i\left(k^*_{R\sigma+}-k_{R\sigma+}\right)x\right]\left[\left(k^*_{R\sigma+}+k_{R\sigma+}\right)-\alpha\chi^+_{R\sigma+}\sigma_y\chi_{R\sigma+}\right] \\
+\left(t^*_{1\bar{\sigma}}t_{1,\bar{\sigma}}\right)\exp\left[-i\left(k^*_{R\bar{\sigma}+}-k_{R\bar{\sigma}+}\right)x\right]\left[\left(k^*_{R\bar{\sigma}+}+k_{R\bar{\sigma}+}\right)-\alpha\chi^+_{R\bar{\sigma}+}\sigma_y\chi_{R\bar{\sigma}+}\right] \\
+\left(t^*_{-1\sigma}t_{-1\sigma}\right)\exp\left[-i\left(k^*_{R\sigma-}-k_{R\sigma-}\right)x\right]\left[\left(k^*_{R\sigma-}+k_{R\sigma-}\right)-\alpha\chi^+_{R\sigma-}\sigma_y\chi_{R\sigma-}\right] \\
+\left(t^*_{-1\bar{\sigma}}t_{-1,\bar{\sigma}}\right)\exp\left[-i\left(k^*_{R\bar{\sigma}-}-k_{R\bar{\sigma}-}\right)x\right]\left[\left(k^*_{R\bar{\sigma}-}+k_{R\bar{\sigma}-}\right)-\alpha\chi^+_{R\bar{\sigma}-}\sigma_y\chi_{R\bar{\sigma}-}\right]
\end{array}\right) \\
&+\left(\begin{array}{l}
+\left(t^*_{1\sigma}t_{1,\bar{\sigma}}\right)\exp\left[-i\left(k^*_{R\sigma+}-k_{R\bar{\sigma}+}\right)x\right]\left[\left(k^*_{R\sigma+}+k_{R\bar{\sigma}+}\right)\chi^+_{R\sigma+}\chi_{R\bar{\sigma}+}-\alpha\chi^+_{R\sigma+}\sigma_y\chi_{R\bar{\sigma}+}\right] \\
+\left(t^*_{1\bar{\sigma}}t_{1\sigma}\right)\exp\left[-i\left(k^*_{L\bar{\sigma}+}-k_{L\sigma+}\right)x\right]\left[\left(k^*_{L\bar{\sigma}+}+k_{L\sigma+}\right)\chi^+_{R\bar{\sigma}+}\chi_{R\sigma+}-\alpha\chi^+_{R\bar{\sigma}+}\sigma_y\chi_{R\sigma+}\right] \\
+\left(t^*_{-1\sigma}t_{-1,\bar{\sigma}}\right)\exp\left[-i\left(k^*_{L\sigma-}-k_{L\bar{\sigma}-}\right)x\right]\left[\left(k^*_{L\sigma-}+k_{L\bar{\sigma}-}\right)\chi^+_{L\sigma-}\chi_{L\bar{\sigma}-}-\alpha\chi^+_{L\sigma-}\sigma_y\chi_{L\bar{\sigma}-}\right] \\
+\left(t^*_{-1\bar{\sigma}}t_{-1\sigma}\right)\exp\left[-i\left(k^*_{R\bar{\sigma}-}-k_{R\sigma-}\right)x\right]\left[\left(k^*_{R\bar{\sigma}-}+k_{R\sigma-}\right)\chi^+_{L\bar{\sigma}-}\chi_{L\sigma-}-\alpha\chi^+_{L\bar{\sigma}-}\sigma_y\chi_{L\sigma-}\right]
\end{array}\right)
\end{aligned}
\tag{3.14}
$$

where the second bracket is the contribution to current density due to the interference of two different k wavefunction which are not orthogonal with each other. Will these terms contribute to current density and be position dependent? We will answer this puzzle in the next chapter.

Chapter 4

Method of electric dipole spin resonance

In this chapter main work is to evaluate time dependent wavefunction and spin-dependent reflection and transmission coefficients with two methods. In the first section, we use one side band approximation approach to solve it for a main influence due to electric field. In second section, we use exact numerical approaches, three terms recursive relation and continue fraction, to solve again to confirm one side band approximation result.

4.1 One side band approximation approach

4.1.1 Time modulated wavefunctions with one side band approximation approach

Over all, in order to get analytic solution, we ignore the $\frac{\alpha}{i}\frac{\partial}{\partial y}\sigma_x$ which is so weak and is discussed in Chapter 2.

We start to consider the electric field effect, the side band may contain evanescent mode, even the wavefunctions are not in the time dependent region. In time-independent region, the wavefunctions in x-direction can be described by the different expressions according to different **energy regimes**, see Fig. 4.1.

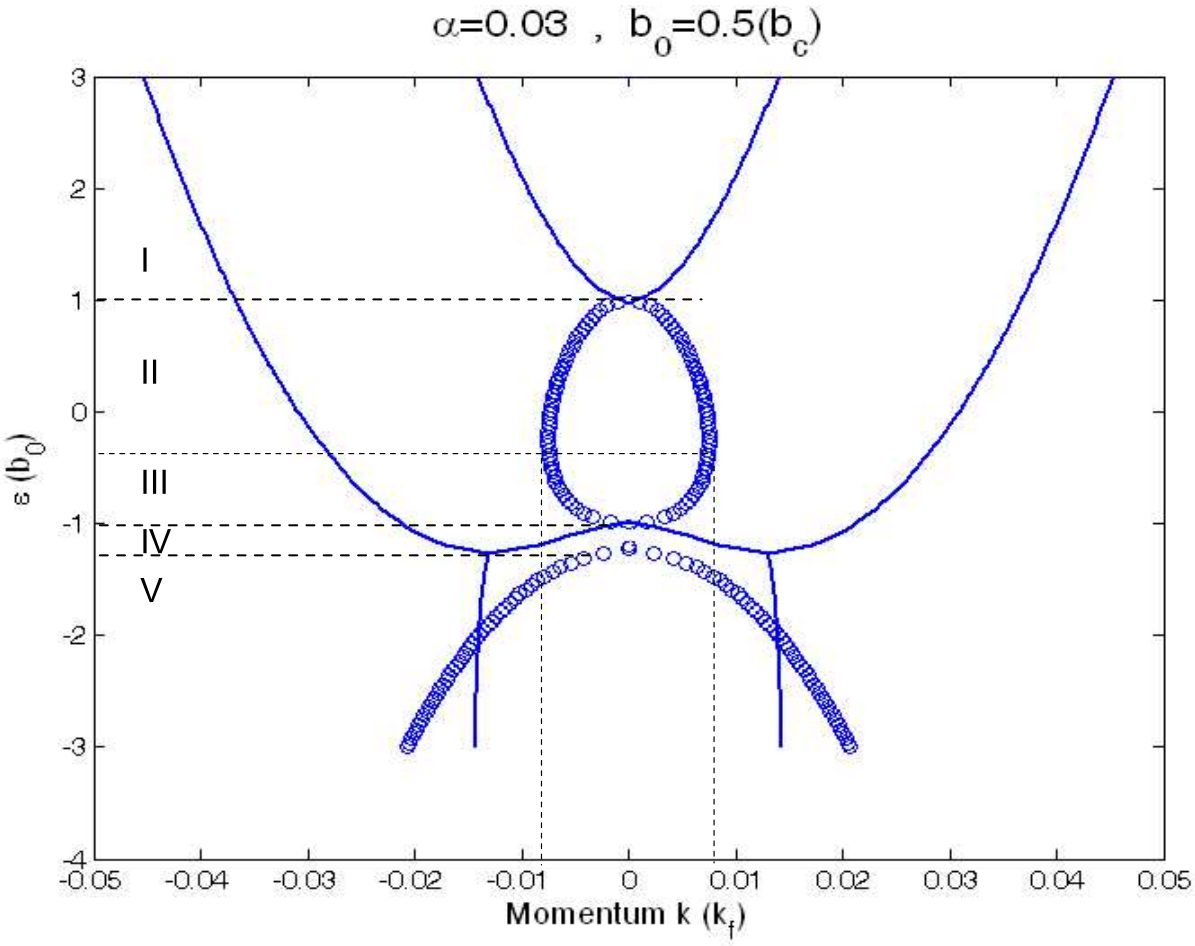

Figure 4.1: We divide the energy into five regimes. The first energy regime is $E > \varepsilon_1 + b_0$, the second is $\varepsilon_1 - (b_0^2/\alpha^2) \leq E < \varepsilon_1 + b_0$ and the critical energy $\varepsilon_1 - b_0^2$ give rise to the maximum pure evanescent momentum, the third is $\varepsilon_1 - b_0 < E < \varepsilon_1 - (b_0^2/\alpha^2)$, the fourth is $\varepsilon_1 - (\alpha^2/4 + b_0^2/\alpha^2) < E < \varepsilon_1 - b_0$, and the last is $E < \varepsilon_1 - (\alpha^2/4 + b_0^2/\alpha^2)$.

Time-independent regions I and III: The wavefunction and energy dispersion can be obtained analytically from Eq. (2.17)

$$\Psi^{I/III} = e^{ikx}\chi_{0R\sigma}e^{-iEt} \tag{4.1}$$

The spin state $\chi_{0R\sigma}$ have different expressions according to different energy regimes, where the first footnote denotes the times of electric inelastic scattering process and the $\pm$ for energy absorb or emit a photon, the second footnote denotes R-ight or L-eft going wave and the third footnote denotes which branch the spin state belong to:

And we transform the energy dispersion into k function of E

$$k(E)^2 = \left[(E-\varepsilon_1) + \frac{\alpha^2}{2}\right] \pm \sqrt{\left((E-\varepsilon_1) + \frac{\alpha^2}{2}\right)^2 - \left((E-\varepsilon_1)^2 - b_0^2\right)} \tag{4.2}$$

Energy regime 1: Energy is above the Zeeman gap, $E > \varepsilon_1 + b_0$,where ε_1 is first energy splitting due to lateral hard wall confining potential and b_0 is the magnetic energy due to external d.c. magnetic field

$$\chi_0 = \frac{1}{\sqrt{2}} \begin{pmatrix} \sigma\frac{b_0+i\alpha k}{\sqrt{b_0^2+\alpha^2k^2}} \\ 1 \end{pmatrix} \tag{4.3}$$

where the four k are all real, $\sigma = +1$ spin states are for outside branch, $\sigma = -1$ spin states are for inside branch where σ is mentioned in Eq. (2.9). And Energy regime 4, $\varepsilon_1 - D < E < \varepsilon_1 - b_0$, $D = \alpha^2/4 + b_0^2/\alpha^2$, the spin states have same expression Eq. (4.3).

Energy regime 2: $\varepsilon_1 - (b_0^2/\alpha^2) \leq E < \varepsilon_1 + b_0$ and the critical energy, $\varepsilon_1 - (b_0^2/\alpha^2)$, give rise to the maximum pure evanescent momentum. For two real momenta k in outside branch, the spin states are the same with Eq. (4.3). For pure image momenta k in inside

branch, the spin state

$$\chi_0 = \frac{\sqrt{b_0 + \alpha Im(k)}}{\sqrt{2b_0}} \begin{pmatrix} \frac{b_0 + i\alpha k}{\sqrt{b_0^2 + \alpha^2 k^2}} \\ 1 \end{pmatrix} \tag{4.4}$$

Energy regime 3: $\varepsilon_1 - b_0 < E < \varepsilon_1 - (b_0^2/\alpha^2)$. For two real momenta k in outside branch, the spin states are the same with Eq. (4.3). For pure imaginary momenta k in inside branch, the spin state

$$\chi_0 = \frac{\sqrt{b_0 + \alpha Im(k)}}{\sqrt{2b_0}} \begin{pmatrix} -\frac{b_0 + i\alpha k}{\sqrt{b_0^2 + \alpha^2 k^2}} \\ 1 \end{pmatrix} \tag{4.5}$$

The signs of spin states with pure imaginary momentum in the Energy regime 2 and Energy regime 3 are opposite. The sign changes suddenly while the energy cross the critical energy $\varepsilon_1 - (b_0^2/\alpha^2)$.

Energy regime 5: For energy under subband bottom, $E < \varepsilon_1 - D$, the spin state is too complicated to distinguish in the diagram which branch does the spin state belong to. But we can know the properties(right or left going decay and inside or outside branch) of complex momentum k by means of expression Eq. (4.2) and substitute k into their own spin state

$$\chi_0 = \left(\frac{\sqrt{b_0^2 - 2b_0\alpha\,\mathrm{Im}(k) + \alpha^2 k^* k}}{\sqrt{b_0^2 + 2b_0\alpha\,\mathrm{Im}(k) + \alpha^2 k^* k}} + 1 \right)^{-1/2} \begin{pmatrix} -\frac{b_0 + i\alpha k}{\frac{\alpha^2}{2} - \sqrt{\left(\Delta + \frac{\alpha^2}{2}\right)^2 - \left(\Delta^2 - b_0^2\right)}} \\ 1 \end{pmatrix} \tag{4.6}$$

where $\Delta = E - \varepsilon_1$ is regarded as kinetic energy.

Position Region II: Time-dependent region, the Hamiltonian is Eq. (3.8) and time modulated wavefunctions have the general expression Eq. (3.9).

In one side band approximation, the scattering process occurs only one time, the first and third expoterms in Eq. (3.9) are eliminated since they involve two photon process.

And the spin state χ have the logistic form

$$\chi = \chi_0 + \chi_{-1}e^{i\omega t} + \chi_{+1}e^{-i\omega t}$$

where $\chi_{\pm 1}$ denotes the spin states whose energy change $\pm\omega$ under one time inelastic scattering process and are evaluated by the following equation

$$\begin{aligned} \begin{pmatrix} \omega - E & i\alpha k + b_0 \\ -i\alpha k + b_0 & \omega - E \end{pmatrix} \chi_{-1} &= i\kappa\sigma_y\chi_0 \\ \begin{pmatrix} -\omega - E & i\alpha k + b_0 \\ -i\alpha k + b_0 & -\omega - E \end{pmatrix} \chi_{+1} &= -i\kappa\sigma_y\chi_0 \end{aligned} \tag{4.7}$$

where $2\kappa \equiv \alpha E_0/\omega$. The system of equations comes from the first order correction to unperturbed spin state χ_0 by means of perturbation theorem. Here we treat the term, $\frac{\alpha E_0}{\omega}\sin(\omega t)\sigma_y$, as perturbation of Eq. (3.8). And it is valid in this criterion $\alpha E_0/\omega^2 < 0.1$ (dimensionless).

Finally we have the time modulated wavefunction in time-dependent region whose one side band approximation as following

$$\Psi^{III}(E) = e^{ikx}\left\{ \begin{array}{l} \chi_0 + \left[\chi_{-1} - i\dfrac{E_0}{\omega^2}k(E)\chi_0\right]e^{i\omega t} \\ + \left[\chi_{+1} - i\dfrac{E_0}{\omega^2}k(E)\chi_0\right]e^{-i\omega t} \end{array} \right\} e^{-iEt} \tag{4.8}$$

4.1.2 Intraband transition and multiple scattering procession

Before we start to calculate reflection and transmission coefficients, we have to emphasize a particular phenomenon that intraband transition in the same subband occurs without breaking symmetry in y-direction. See Fig. 4.2. The reason of why breaking symmetry in y-direction is not necessary for the transition between difference branch in the same subband is the external magnetic field mix the two spin state of σ_y and σ_x due to Rashba effect and external magnetic field. Therefore the orthogonality between different branch

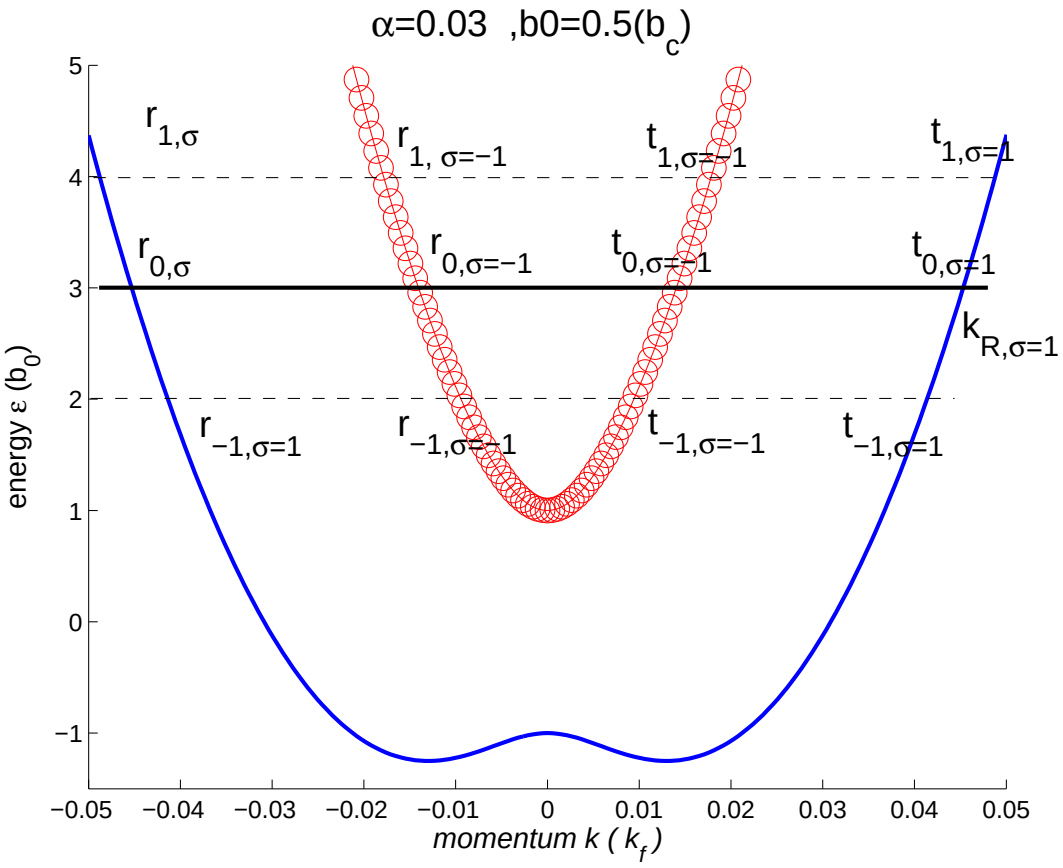

Figure 4.2: Sketch of intraband transition, without breaking symmetry in y-direction, rises from mixing spin states of Rashba and Zeeman terms due to an external magnetic field $\mathbf{B}(\hat{x})$. Where $k_{R\sigma}$ denotes the momentum of an incident wave; $r_{\pm1,\pm1}$ is the reflection coefficients of once scattering to specific one branch; Because of no two photon scattering process, the $r_{0,\pm1}$ the $r_{2,\pm1}$ are zero. The solid horizontal line denote incident energy; the dashed line for the energy after inelastic scattering process.

in the same subband disappears. Because of this reason, the intraband transition process is allowed.

We can start to calculate reflection and transmission coefficients by multiple scattering process which is the matching calculation at each interface step by step. Besides, all scattering process is considered up to the first order only. In other words, we ignore the second order process including:

1. Successive scatter to $E + 2\omega$ at one interface. (minus sign also)
2. First scatter to $E + \omega$ and then back to E at one interface. (minus sign also)
3. First scatter to $E+\omega$ at one interface and then to $E+2\omega$ at the other interface. (minus sign also)

Finally, we sum all contribution of the same energy level and branch from two interface, see Fig. 4.3.

4.1.3 Reflection and transmission coefficients

Our aim is to solve the reflection and transmission coefficients by the imposed boundary conditions: (i) wave functions are continuous at $x = 0$ `and` $x = l$. (ii) the slope of wave functions are continuous at $x = 0$ `and` $x = l$.

(i)

$$\begin{cases} \Psi^I(0^-) = \Psi^{II}(0^+) \text{ at first interface} \\ \Psi^{II}(l^-) = \Psi^{III}(l^+) \text{ at second interface} \end{cases} \tag{4.9}$$

(ii)

$$\begin{cases} -\frac{\partial}{\partial x}\Psi\Big|_{0^-}^{0^+} + i\frac{E_0}{\omega}\sin(\omega t)\Psi(0) = 0 \text{ at first interface} \\ -\frac{\partial}{\partial x}\Psi\Big|_{l^-}^{l^+} - i\frac{E_0}{\omega}\sin(\omega t)\Psi(l) = 0 \text{ at second interface} \end{cases} \tag{4.10}$$

The wavefunctions in each position region have been introduced by Eq. (4.1) and Eq. (4.8).

And these boundary conditions necessarily are satisfied at arbitrary time. Therefore we can evaluate the coefficients with three different energy levels, $E, E \pm \omega$, separately. Besides, Eq. (4.9) and Eq. (4.10) are two components wavefunction. So the four equations give us 24 equations which can exactly solve out 24 unknown variables. There are 12 unknown variables of reflection shown in Fig. 4.2 with respect to one of interfaces.

After conventional matching calculation, we obtain the expression, i.e. case1.1 [$k_{R\sigma}$ incident and at first interface] , for reflection and transmission coefficients of up(down) energy level

$$\begin{pmatrix} A_{0L\sigma k\pm} & A_{0L\bar{\sigma}k\pm} & -A_{0R\sigma k\pm} & -A_{0R\bar{\sigma}k\pm} \\ B_{0L\sigma k\pm} & B_{0L\bar{\sigma}k\pm} & -B_{0R\sigma k\pm} & -B_{0R\bar{\sigma}k\pm} \\ k_{L\sigma\pm}A_{0L\sigma k\pm} & k_{L\bar{\sigma}\pm}A_{0L\bar{\sigma}k+} & -k_{R\sigma\pm}A_{0R\sigma k\pm} & -k_{R\bar{\sigma}\pm}A_{0R\bar{\sigma}k\pm} \\ k_{L\sigma\pm}B_{0L\sigma k\pm} & k_{L\bar{\sigma}\pm}B_{0L\bar{\sigma}k+} & -k_{R\sigma\pm}B_{0R\sigma k\pm} & -k_{R\bar{\sigma}\pm}B_{0R\bar{\sigma}k\pm} \end{pmatrix} \begin{pmatrix} r_{\pm 1\sigma} \\ r_{\pm 1\bar{\sigma}} \\ t_{\pm 1\sigma} \\ t_{\pm 1\bar{\sigma}} \end{pmatrix} = \begin{pmatrix} \tilde{A}_{+1R\sigma} - i\frac{E_0}{\omega^2}k_{R\sigma}\tilde{A}_{0R\sigma} \\ \tilde{B}_{+1R\sigma} - i\frac{E_0}{\omega^2}k_{R\sigma}\tilde{B}_{0R\sigma} \\ \mp i\frac{E_0}{2\omega}\tilde{A}_{0R\sigma} + k_{R\sigma}\left(\tilde{A}_{+1R\sigma} - i\frac{E_0}{\omega^2}k_{R\sigma}\tilde{A}_{0R\sigma}\right) \\ \mp i\frac{E_0}{2\omega}\tilde{B}_{0R\sigma} + k_{R\sigma}\left(\tilde{B}_{+1R\sigma} - i\frac{E_0}{\omega^2}k_{R\sigma}\tilde{B}_{0R\sigma}\right) \end{pmatrix} \tag{4.11}$$

as well as case1.2 [$k_{R\sigma}$ incident and at second interface] , for reflection and transmission coefficients of up(down) energy level

$$\begin{pmatrix} A_{0L\sigma\pm} & A_{0L\bar{\sigma}\pm} & -A_{0R\sigma\pm} & -A_{0R\bar{\sigma}\pm} \\ B_{0L\sigma\pm} & B_{0L\bar{\sigma}\pm} & -B_{0R\sigma\pm} & -B_{0R\bar{\sigma}\pm} \\ (k_{L\sigma\pm})\,A_{0L\sigma\pm} & (k_{L\bar{\sigma}\pm})\,A_{0L\bar{\sigma}\pm} & -(k_{R\sigma\pm})\,A_{0R\sigma\pm} & -(k_{R\bar{\sigma}\pm})\,A_{0R\bar{\sigma}\pm} \\ (k_{L\sigma\pm})\,B_{0L\sigma\pm} & (k_{L\bar{\sigma}\pm})\,B_{0L\bar{\sigma}\pm} & -(k_{R\sigma\pm})\,B_{0R\sigma\pm} & -(k_{R\bar{\sigma}\pm})\,B_{0R\bar{\sigma}\pm} \end{pmatrix} \begin{pmatrix} r_{\pm 1\sigma}\exp(ik_{L\sigma\pm}l) \\ r_{\pm 1\bar{\sigma}}\exp(ik_{L\bar{\sigma}\pm}l) \\ t_{\pm 1\sigma}\exp(ik_{R\sigma\pm}l) \\ t_{\pm 1\bar{\sigma}}\exp(ik_{R\bar{\sigma}\pm}l) \end{pmatrix}$$

$$= \begin{pmatrix} -\exp(ik_{R\sigma}l)\left[\left(\tilde{A}_{+1,R,\sigma}\right) - i\frac{E_0}{\omega^2}k_{R\sigma}\left(\tilde{A}_{0R\sigma}\right)\right] \\ -\exp(ik_{R\sigma}l)\left[\left(\tilde{B}_{+1,R,\sigma}\right) - i\frac{E_0}{\omega^2}k_{R\sigma}\left(\tilde{B}_{0R\sigma}\right)\right] \\ -\exp(ik_{R\sigma}l)\left(\mp i\frac{E_0}{2\omega}\tilde{A}_{0R\sigma} + (k_{R\sigma})\left[\tilde{A}_{+1,R,\sigma} - i\frac{E_0}{\omega^2}k_{R\sigma}\tilde{A}_{0R\sigma}\right]\right) \\ -\exp(ik_{R\sigma}l)\left(\mp i\frac{E_0}{2\omega}\tilde{B}_{0R\sigma} + (k_{R\sigma})\left[\tilde{B}_{+1,R,\sigma} - i\frac{E_0}{\omega^2}k_{R\sigma}\tilde{B}_{0R\sigma}\right]\right) \end{pmatrix} \tag{4.12}$$

where upper(lower) sign is denoted for up(down) side band energy, A and B are two elements of spin state and the tilde sign in $\tilde{A}$ or $\tilde{B}$ mean the energy level remain at E, the same with incident wave energy, and the $\pm$ sign in $k_{\pm}$ means the energy in Eq. (4.2) absorb or emit one photon energy.

Here are similar results as follow we do not show for a short make-up,

case2.1 [$k_{R-\sigma}$ incident and at first interface],

case2.2 [$k_{R-\sigma}$ incident and at second interface].

Until now, the coefficient t_0 is not mentioned since it contain second order correction. It can not be obtained by one side band approach method previous mentioned. But it can be calculated by an indirect method. Through the conservation of number current flow identity

$$J_{in} = J_R + J_T \tag{4.13}$$

where J_{in} is the incident current flow, J_R is reflection current flow and J_T is the transmission current flow.

Therefore the calculation of number current flow is introduced in the next section.

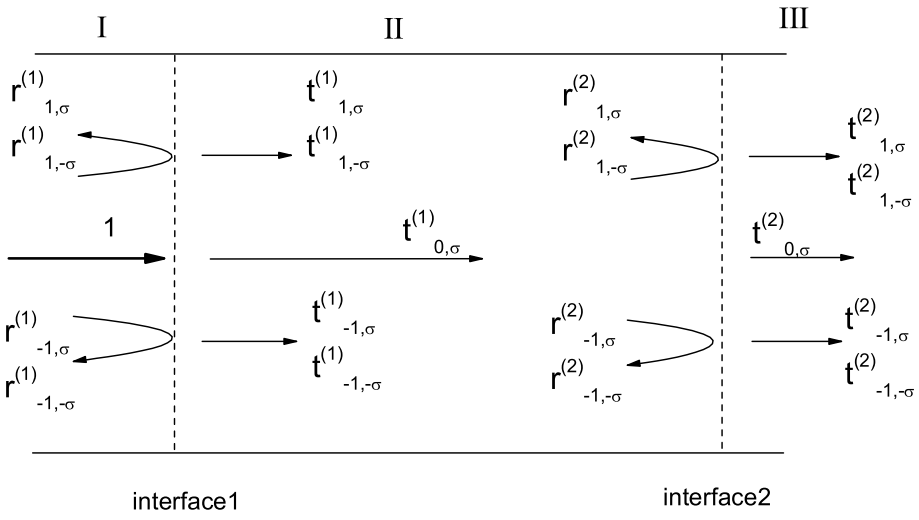

Figure 4.3: Sketch of multiple scattering procession in order to evaluate reflection and transmission coefficients. For example, $k_{R\sigma}$ wave incident, the reflection comes from both interfaces $r_{\pm1,\pm\sigma} = r^{(1)}_{\pm1,\pm\sigma} + r^{(2)}_{\pm1,\pm\sigma}$. The upper index denotes the first interface (1) and the second interface (2). $r_{2,\pm\sigma} = 0$ are not shown in this figure.

Actually, by means of this conservation identity we just obtain $|t_0|^2$, the magnitude square of the t_0 coefficient.

4.1.4 Revisit particle current density

The wavefunctions in each region are introduced in the previous section as well as reflection and transmission coefficients considered up to one side band. Now we can use them to evaluate particle current.

The particle current operator can be calculated from "continuity equation" and the particle current flow can be written as Eq. (3.11) For an example, we calculate particle current flow with the wavefunction $\Psi(\mathbf{r},t) = \exp(ik_{R\sigma}x)\phi_n(y)\chi_{0R\sigma}\exp(-Et)$ where

$$\chi_{0R\sigma} = \frac{1}{\sqrt{2}} \begin{pmatrix} -\sigma \frac{b_0 + i\alpha k_{R\sigma}}{\sqrt{b_0^2 + \alpha^2 k_{R\sigma}^2}} \\ 1 \end{pmatrix} \tag{4.14}$$

Substituting the wave function into Eq. (3.12), we can obtain the current flow

$$J(x,t) = 2k_{R\sigma} - \sigma \frac{\alpha^2 k_{R\sigma}}{\sqrt{b_0^2 + \alpha^2 k_{R\sigma}^2}} \tag{4.15}$$

The result can be demonstrated by derivative the energy dispersion Eq. (2.9) with respect to k, dE/dk . It turns out group velocity expression which is same with Eq. (4.15).

Therefore we can answer the question we asked in the Chapter 3 "Will these interference terms between different wavefunction which are not orthogonal with each other contribute to current density? "

This is easy to answer the question by substituting spin states Eq. (4.3)$\sim$ Eq. (4.6) into Eq. (4.16) to demonstrate what role these cross terms play but the calculation process is very complicated and boring. Here we just justify that the cross terms contribute NOTHING to the current density in any energy regime, even all momenta k are propagating mode. Therefore Eq. (3.14) can be reduced to

$$\begin{aligned}
&\frac{1}{T}\int_0^T J(x,t)dt = \\
&\left(\begin{array}{l}
\exp\left[i\left(k_{0R\sigma} - k_{0R\sigma}^*\right)x\right]\left[\left(k_{0R\sigma}^* + k_{0R\sigma}\right) - \alpha\chi_{0R\sigma}^\dagger \sigma_y \chi_{0R\sigma}\right] \\
+ \left(r_{1\sigma}^* r_{1\sigma}\right)\exp\left[-i\left(k_{+1L\sigma}^* - k_{+1L\sigma}\right)x\right]\left[\left(k_{+1L\sigma+}^* + k_{+1L\sigma}\right) - \alpha\chi_{+1L\sigma}^\dagger \sigma_y \chi_{+1L\sigma}\right] \\
+ \left(r_{1\bar{\sigma}}^* r_{1,\bar{\sigma}}\right)\exp\left[-i\left(k_{+1L\bar{\sigma}}^* - k_{+1L\bar{\sigma}}\right)x\right]\left[\left(k_{+1L\bar{\sigma}}^* + k_{+1L\bar{\sigma}}\right) - \alpha\chi_{+1L\bar{\sigma}}^\dagger \sigma_y \chi_{+1L\bar{\sigma}}\right] \\
+ \left(r_{-1\sigma}^* r_{-1\sigma}\right)\exp\left[-i\left(k_{-1L\sigma}^* - k_{-1L\sigma}\right)x\right]\left[\left(k_{-1L\sigma}^* + k_{-1L\sigma}\right) - \alpha\chi_{-1L\sigma}^\dagger \sigma_y \chi_{-1L\sigma}\right] \\
+ \left(r_{-1\bar{\sigma}}^* r_{-1,\bar{\sigma}}\right)\exp\left[-i\left(k_{-1L\bar{\sigma}}^* - k_{-1L\bar{\sigma}}\right)x\right]\left[\left(-1k_{L\bar{\sigma}}^* + k_{-1L\bar{\sigma}}\right) - \alpha\chi_{-1L\bar{\sigma}}^\dagger \sigma_y \chi_{-1L\bar{\sigma}}\right]
\end{array} \right)
\end{aligned} \tag{4.16}$$

When all momenta are real, it is obvious the result of particle current is not position-dependent. Besides, it is easy to demonstrate that the current is not position-dependent by substituting proper spin states when all momenta are not real.

4.2 Exact numerical approach

In this section, exact numerical approaches [14], three-term recursive relation and continued fraction, are introduced here. we start from the Hamiltonian

$$\left\{ \begin{pmatrix} 0 & b_0 + i\alpha k \\ b_0 - i\alpha k & 0 \end{pmatrix} + \frac{\alpha E_0}{\omega} \sin(\omega t) \begin{pmatrix} 0 & -i \\ i & 0 \end{pmatrix} \right\} \chi = i\frac{\partial}{\partial t}\chi \tag{4.17}$$

We define $\gamma \equiv (b_0 + i\alpha k)$ and $\kappa \equiv \frac{\alpha E_0}{2\omega}$ and expand spin state χ as Fourier expansion

$$\chi = \begin{pmatrix} A \\ B \end{pmatrix} = e^{i\varepsilon t} \begin{pmatrix} \sum_n A_n e^{in\omega t} \\ \sum_n B_n e^{in\omega t} \end{pmatrix} \tag{4.18}$$

where n is integral and ε is an undetermined constant which is not necessary to be the incident energy. Substituting Eq. (4.18) into Eq. (4.17), we have a system of equations

$$\begin{cases} [\gamma - \kappa(e^{i\omega t} - e^{-i\omega t})] \sum_n B_n e^{in\omega t} = -(\varepsilon + n\omega) \sum_n A_n e^{in\omega t} \\ [\gamma^* + \kappa(e^{i\omega t} - e^{-i\omega t})] \sum_n A_n e^{in\omega t} = -(\varepsilon + n\omega) \sum_n B_n e^{in\omega t} \end{cases} \tag{4.19}$$

The $e^{-i\omega t}$ terms in the system of equation are

$$\begin{cases} \gamma B_n - \kappa B_{n-1} + \kappa B_{n+1} = -(\varepsilon + n\omega) A_n \\ \gamma^* A_n + \kappa A_{n-1} - \kappa A_{n+1} = -(\varepsilon + n\omega) B_n \end{cases} \tag{4.20}$$

The two equations have very similar formulism and the ansatz, $B_n = (-1)^n A_n^*$, is suggested which satisfies with the both of Eq. (4.20).

Substituting it into the first equation of Eq. (4.20), we can obtain the three terms recursive relation of B_n

$$\gamma B_n - \kappa B_{n-1} + \kappa B_{n+1} = -(-1)^n (\varepsilon + n\omega) B_n^* \tag{4.21}$$

The Eq. (4.21) can be represented by continuous fraction of B

$$\frac{B_n}{B_{n-1}} = \frac{\kappa}{\gamma + (-1)^n (\varepsilon + n\omega) \frac{B_n^*}{B_n} + \kappa \frac{B_{n+1}}{B_n}} \tag{4.22}$$

For very large $n = N$, this is a very small probability for an electron to excite to such high energy level. Therefore $\frac{B_{N+1}}{B_N}$ can be ignore in order to obtain the approximation

$$\vartheta_N = \frac{-(-1)^N (\varepsilon + N\omega)}{\gamma - \kappa \frac{B_{N-1}}{B_N}} \tag{4.23}$$

where $\vartheta_N = \frac{B_N}{B_N^*}$ is the twice of azimuth of B_N. Therefore $\frac{B_n}{B_{n-1}}$ is known and substituted into Eq. (4.22) of $n = N - 1$. And we iterate the process until $n = 0$. On the other hand, we can perform the iterating process from $n = -N$ to $n = 0$. The two iterating processes is sufficient to determinate the value of ε mentioned in Eq. (4.18)

So far, one(or not only one) undeterminate value(s) remained in the iteration is(are) the azimuth of B_n. But Eq. (4.17) is a first order differential equation with two components. Since that, two undeterminate parameter are necessary, i.e. one is ε and the other is the azimuth of B_n. It turns out that the ϑ_n is not n dependent. And how to determinate the value of ϑ is the same with that of ε.

In principle, one can employ this way to solve the solution Eq. (4.18) of Eq. (4.17).

Chapter 5

Results and discussions

In this chapter, the basic and important result is energy dispersion and is introduced in the first section. The following are time dependent numerical results of one side band approach which contain transmission, beat of spin density and number density and spin flip resonance.

5.1 The energy dispersion

The energy dispersions which contain propagating mode and evanescent mode are basic results of this mesoscopic system. They have been introduced in the Fig. 2.5 ∽ Fig. 2.7 in the Section 2.2. We especially focus on the condition of magnetic field strength is comparable with SOI energy and Fig. 2.5 is such important that the following time-dependent results can not be interpreted without it.

5.2 Numerical results of one side band approach

5.2.1 Transmission

The first result of one side band approximation is the total transmission T obtained from number current continuity Eq. (4.13).

$$T = \frac{J_T}{J_{in}} \tag{5.1}$$

where particle currents J_{in} and J_T are calculated by Eq. (4.16). And the result is shown in the Fig. 5.1. The first arrow indicates that an electron with energy $E = -0.5(b_0)$ absorbs a photon with energy $\omega = 1.5(b_0)$ and excites to energy level $E = 1(b_0)$, see Fig. 2.5, which has larger density of state[15]. When electron is trapped, the transmission dip appears. For the same reason, the second arrow indicates that an electron with energy $E = 0.25(b_0)$ emits a photon with energy $\omega = 1.5(b_0)$ and transmits to energy level $E = -1.25(b_0)$. And the third arrow indicates that an electron with energy $E = 0.5(b_0)$ emits a photon with energy $\omega = 1.5(b_0)$ and transmits to energy level $E = -1(b_0)$. And the fourth arrow indicates that an electron with energy $E = 2.5(b_0)$ emits a photon with energy $\omega = 1.5(b_0)$ and transmits to energy level $E = 1(b_0)$.

5.2.2 Spatial beat patterns of spin density and particle density

In the previous chapter, the wavefunction and coefficients in the region III are obtained and now the spin density can be evaluated by the means of the expectation value of Pauli matrix, σ_{0xyz}. Particularly to mention that the expectation value of $\sigma_0 = 1$ denotes particle density.

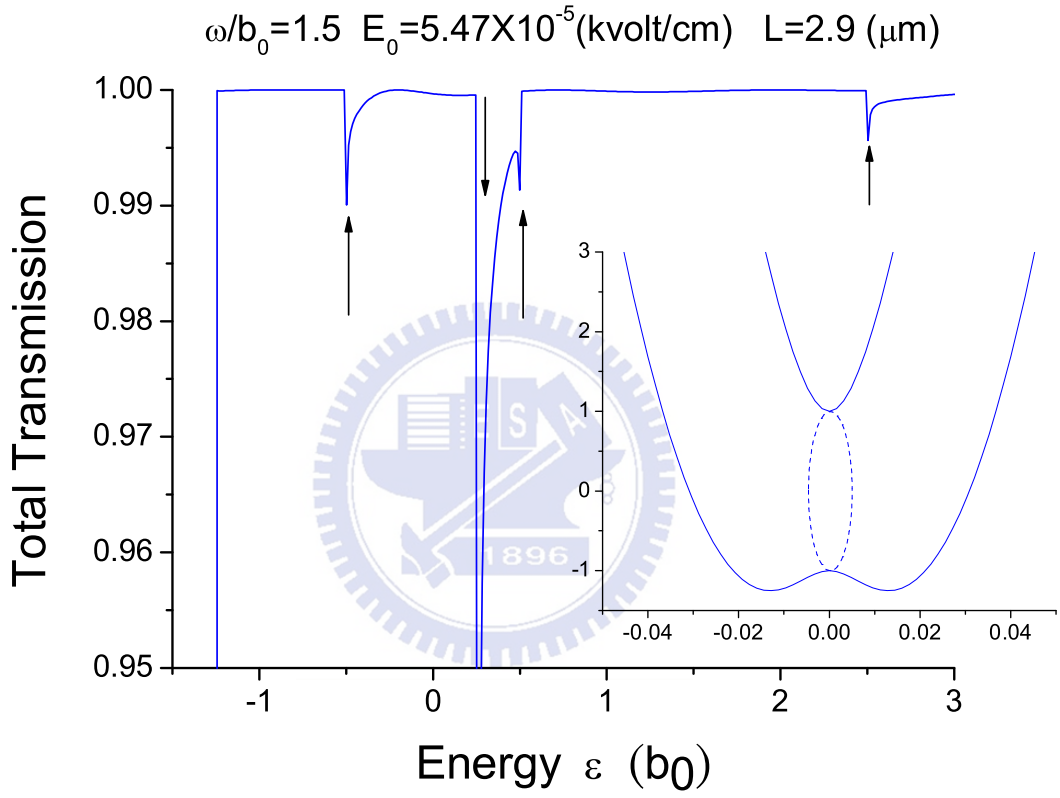

Figure 5.1: The transmission dips appear when the first side band involves the top and bottom of Zeeman gap or subband bottom(shown in the inserted plot), i.e. which are states with larger density of state. The ω/b_0 indicates the photon energy is in unit of b_0, the L is the length of time modulated region and ε_1 is the first spitting energy due to lateral confinement.

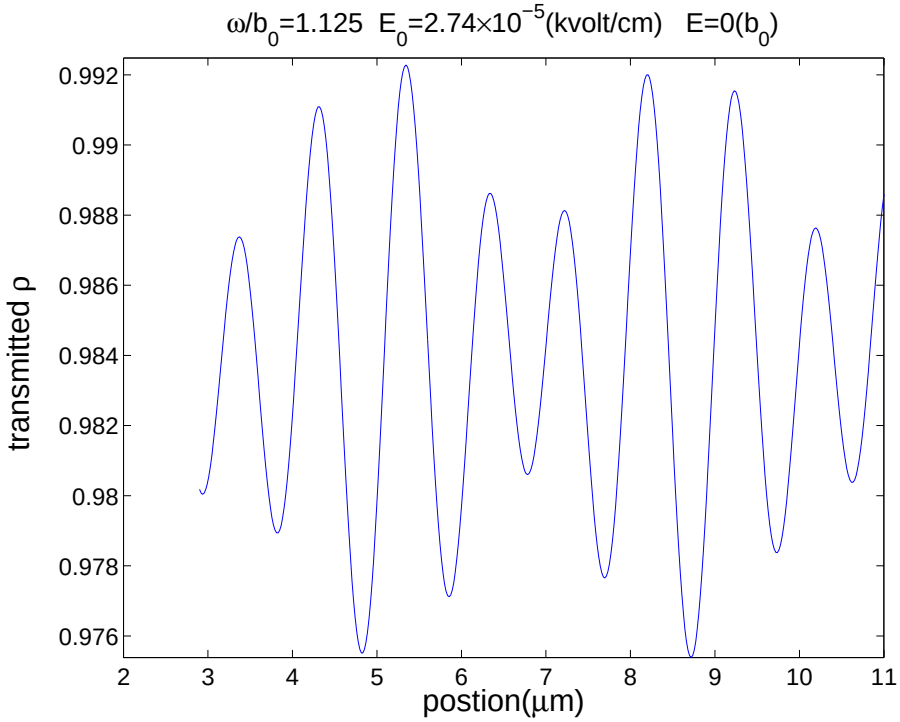

Figure 5.2: Beat pattern of transmitted number density in regione III with $4\mu m$ periodicity.

The difference between the two interferences of up and down side bands

$$2\,\mathrm{Re}\left(\left\langle t_{1\sigma}\psi(k_{R\sigma+})\right|\sigma_i\left|t_{1\bar{\sigma}}\psi(k_{R\bar{\sigma}+})\right\rangle\right)$$

$$and \qquad\qquad where\ \ i=0,x,y,z$$

$$2\,\mathrm{Re}\left(\left\langle t_{-1\sigma}\psi(k_{R\sigma-})\right|\sigma_i\left|t_{-1\bar{\sigma}}\psi(k_{R\bar{\sigma}-})\right\rangle\right)$$

give rise to oscillating beat pattern, see Fig. 5.2 and Fig. 5.3. Generally speaking, in the condition of the coefficients t_{+1} and t_{-1} are comparable, the obvious beat pattern occurs when $\Delta k = |\delta k_+ - \delta k_-|$ is large where $\delta k_+ = |k_{+\sigma}(E+\omega) - k_{-\sigma}(E+\omega)|$ and $\delta k_- = |k_{+\sigma}(E-\omega) - k_{-\sigma}(E-\omega)|$ and the σ denotes branch index. The reason for the interference appearance is that the magnetic field mix the two branch of bare Rashba energy spectrum. Therefore the two branch are not orthogonal any more and the interference terms survive. And periodicity of density can be proposed to measure coherent length. [16]. The length of beat pattern is the coherent length of this mesoscopic system.

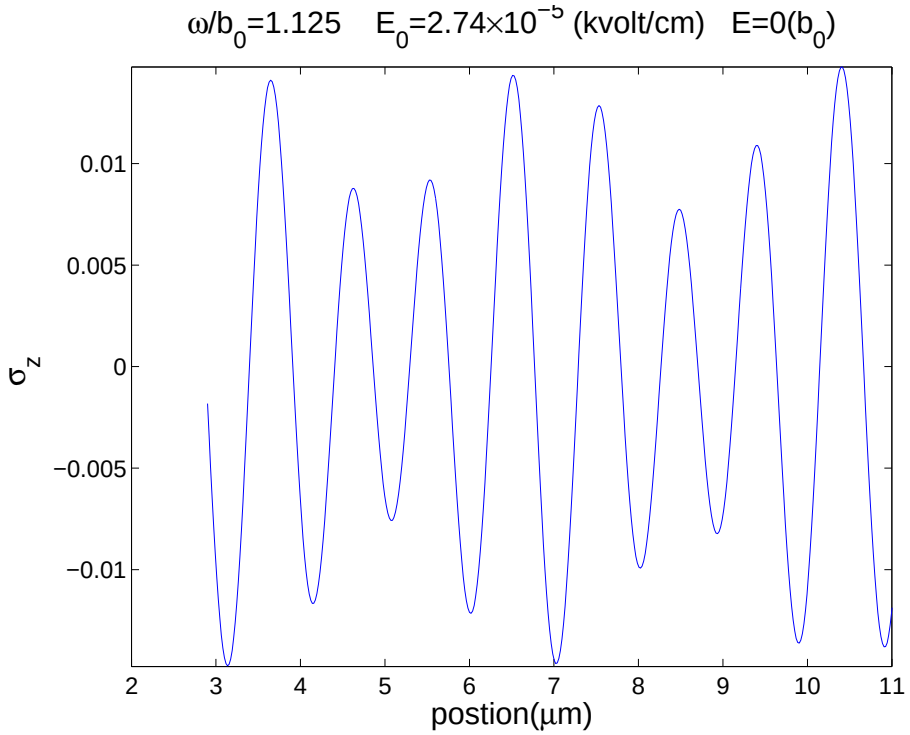

Figure 5.3: Beat pattern of transmitted spin density of σ_z in regione III with $4\mu m$ periodicity.

5.2.3 Spin flip resonance

The concept of this section is analog to conventional nuclear magnetic resonance(NMR). In NMR, the resonance occurs while the electron in one specific spin state emits or absorb a photon with energy ω and then flip the spin state into the other spin state. The photon energy ω matches the energy difference between the two spin states. Besides the two states both have large density od state. In this thesis, the resonance is indicated by the wavefunction $\psi_{\pm\omega-\sigma}$. The magnitude square of these wavefunctions stand for the probability of transition to the branch labelled by $-\sigma$ which is different with that labelled by σ of incident wave. These two branches, $\pm\sigma$ have different spin states respectively mentioned in Chapter 4. The resonance result is shown in the Fig. 5.4 $\sim$ Fig. 5.6. In these figures, the incident wave comes from the σ branch. The resonance peaks of $|\psi_{\pm\omega-\sigma}|^2$ indicate that transition trend to change spin state while side band involve the states which have larger density of state. This configuration is analog to conventional MNR condition

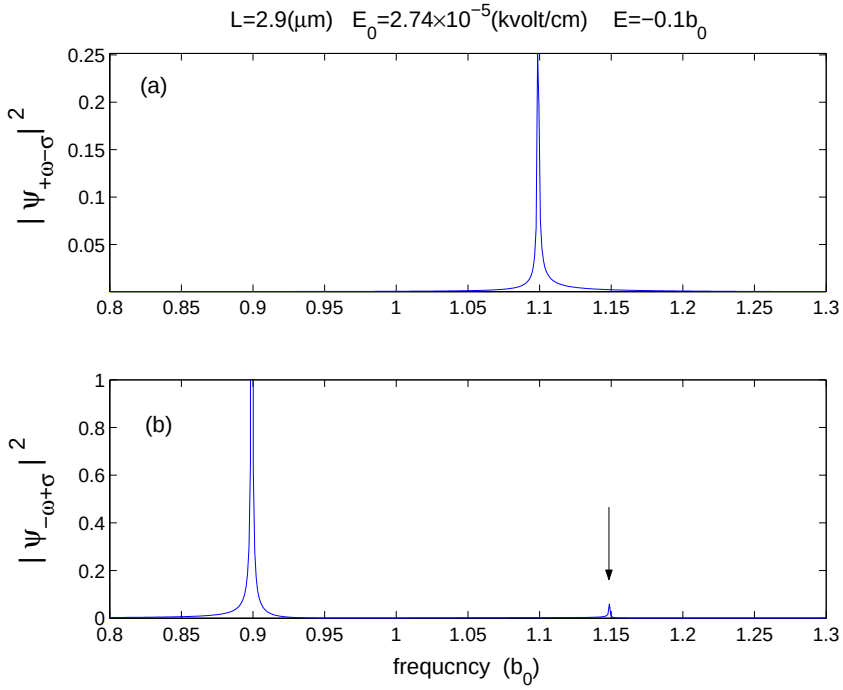

Figure 5.4: Incident wave comes from σ branch and the magnitude square of $\psi_{\pm\omega-\sigma}$ is the probability of changing branch(spin flip).

of two discrete state also.

In the panel (b) of Fig. 5.4 $\sim$ Fig. 5.6, arrows point out a small resonance peak. These arrows appear at higher frequency ω i.e. higher photon energy. This higher frequency makes the time modulated term $\frac{\alpha E_0}{w}\sin(\omega t)\sigma_y$ in Eq. (3.8) too small to be side band mechanism any more. Therefore a smaller resonance appears.

5.3 More discussions

Over all, the time modulated electric field strength is 10^{-5} order in unit of $kvolt/cm$. Actually this magnitude is such small. This limitation comes from one side band approximation which must ignore two photon scattering process and high order correction to wavefunction.

Second, Fig. 5.7 shows the SD_z standard deviations of spin density σ_z is always larger then SD_n that of particle density. At a.c. electric field length, $L = 2.9\mu m$, it is a optimal

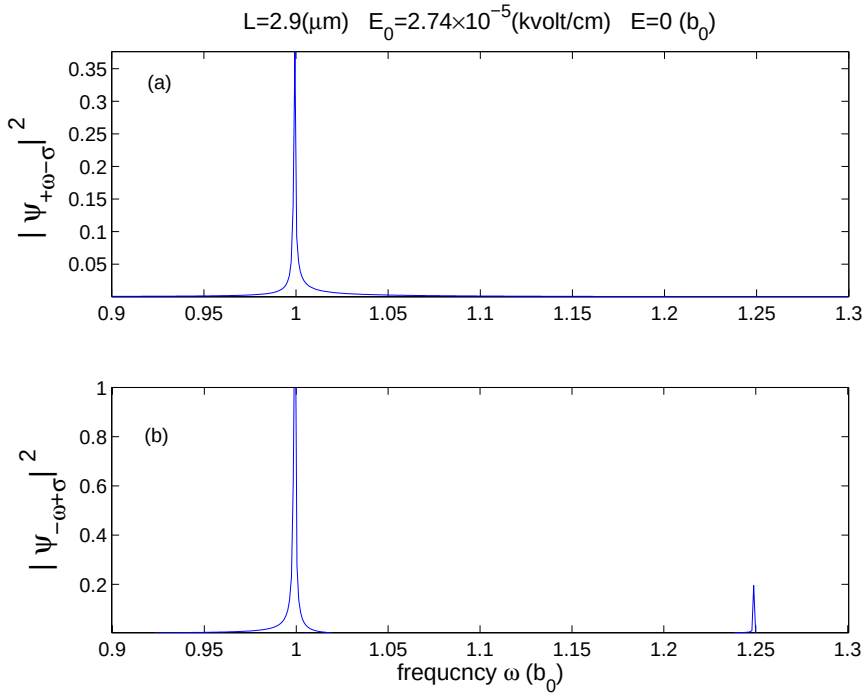

Figure 5.5: Incident wave comes from σ branch and the magnitude square of $\psi_{\pm\omega-\sigma}$ is the probability of changing branch(spin flip).

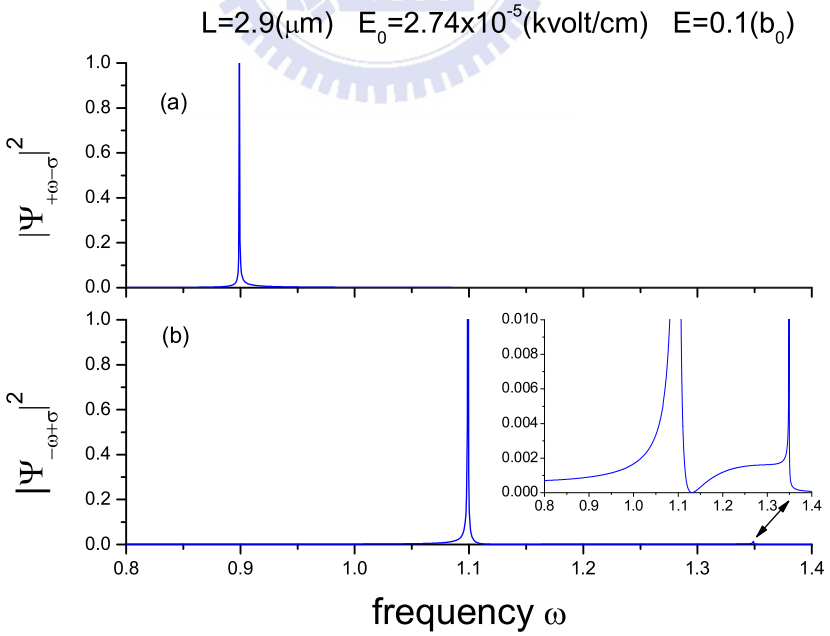

Figure 5.6: Incident wave comes from σ branch and the magnitude square of $\psi_{\pm\omega-\sigma}$ is the probability of changing branch(spin flip). The inserted plot in (b) is a re-scale view of small peak at $\omega = 1.35$.

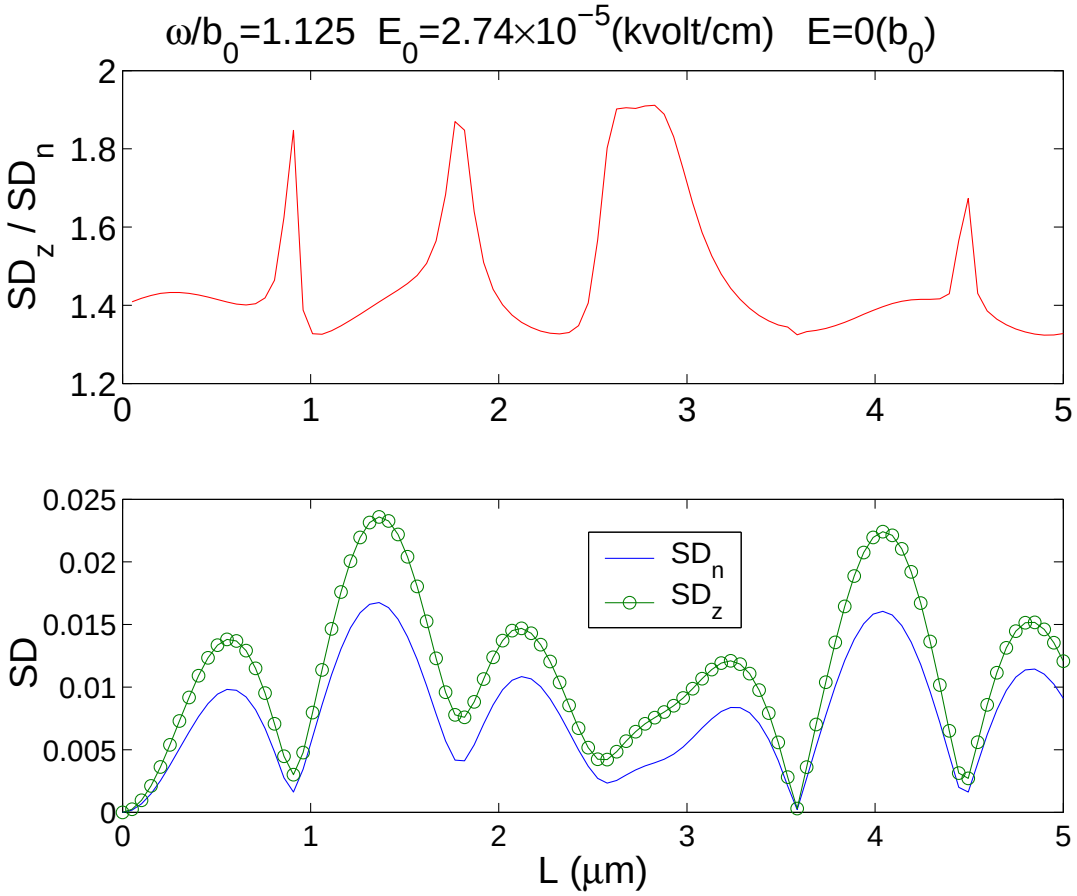

Figure 5.7: Standard deviations show that $SD_z > SD_n$ to guarantee that it is not necessary to consider screening correction. At length of a.c. electric field is $L = 2.9\mu m$, the ratio between them is almost twice.

condition that SD_z almost is twice of SD_n. The result indicates that it is not necessary to consider about screening correction.

Third, all fields including external static magnetic, time modulated electric field and induced magnetic field due to Rashba type SOI are in-plane fields. By intuition, spin precession axis is in-plain and the expectation value of σ_z should be zero. But Fig. 5.3 does not agree and show the evidence of spin flip. It can be interpreted by a semi-classical picture. In conventional NMR configuration and in rotating frame with frequency which is the same with external rotating magnetic field B_{rot}, the spin performs precession about B_{rot} instead of static magnetic field B_s, see Fig. 5.8.

Finally, Boundary conditions, Eq. (4.9) and Eq. (4.10) are spin- independent in in-

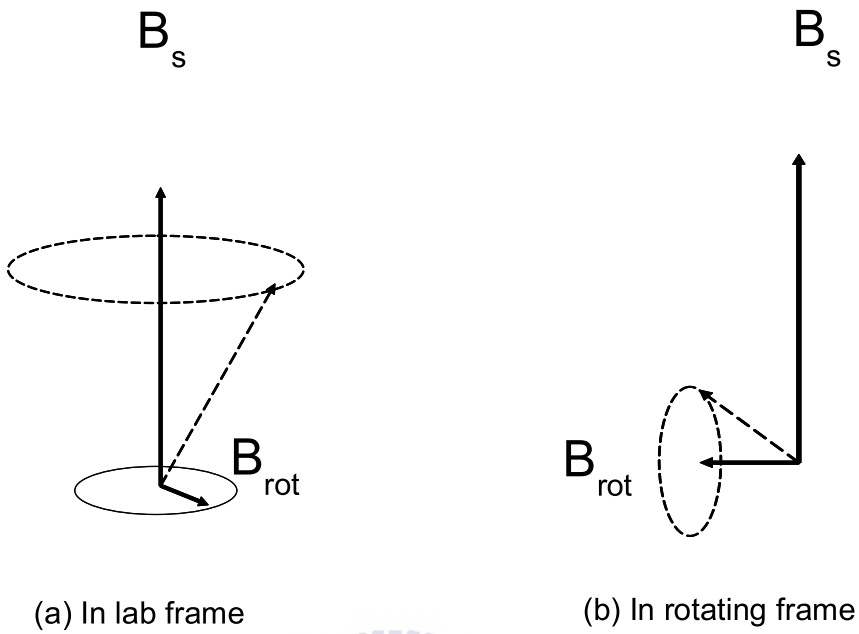

Figure 5.8: The resonance occurs and spin flip that can be interpreted by rotating frame with semi-classical picture. Where B_S is static magnetic field and B_{rot} is rotating magnetic field. The dashed line indicates spin and precession.

elastic scattering process. If incident wave comes from branch σ then it is impossible to $t_{\pm\omega-\sigma} \neq 0$ unless the spin flip due to EDSR.

Chapter 6

Future work

In the future, two incident waves coming from two different branches condition will be considered and the one sideband approximation will be extend to exact numerical method mentioned in section 4.2 in order to simulate realistic physics and explore new possible to enhance effects.

The analysis and physical interpretation of fano profile shown in the Fig. 5.6 are in progress.

Appendix A

Review of nuclear magnetic resonance and sideband

Let we review nuclear magnetic resonance(NMR). The configuration of fields of NMR is composed of B_1 static magnetic field along z axis and $B_2(t)$ rotating field in $x-y$ plane. The time-dependent Schrödinger equation of this configuration is described as

$$H\chi = i\frac{\partial}{\partial t}\chi \tag{A.1}$$

where $H = B_2\cos(\omega t)\sigma_x + B_2\sin(\omega t)\sigma_y + B_1\sigma_z$ and χ is a spin state. The analytically general solution can be solved as following

$$\chi(t) = \begin{pmatrix} \exp(-iB_1 t)\left[c_1\exp\left(\frac{i}{2}\beta_+ t\right) + c_2\exp\left(\frac{i}{2}\beta_- t\right)\right] \\ -\frac{\exp(iB_1 t)\exp(-i\beta t)}{2B_2}\left[\beta_+ c_1\exp\left(\frac{i}{2}\beta_+ t\right) + \beta_- c_2\exp\left(\frac{i}{2}\beta_- t\right)\right] \end{pmatrix} \tag{A.2}$$

where c_1 and c_2 are two undeterminate coefficients which can be determinanted by an initial condition, $\beta_\pm = \beta \pm \sqrt{\beta^2 + 4B_2^2}$, $\beta = 2B_1 - \omega$ and ω is angular frequency of B_2 rotating field.

If the initial state of $\chi(0) = [1\ \ 0]^T$ is employed then the evaluation in time of probability of the spin-down state $[0\ \ 1]^T$, called $P_\downarrow(t)$, is

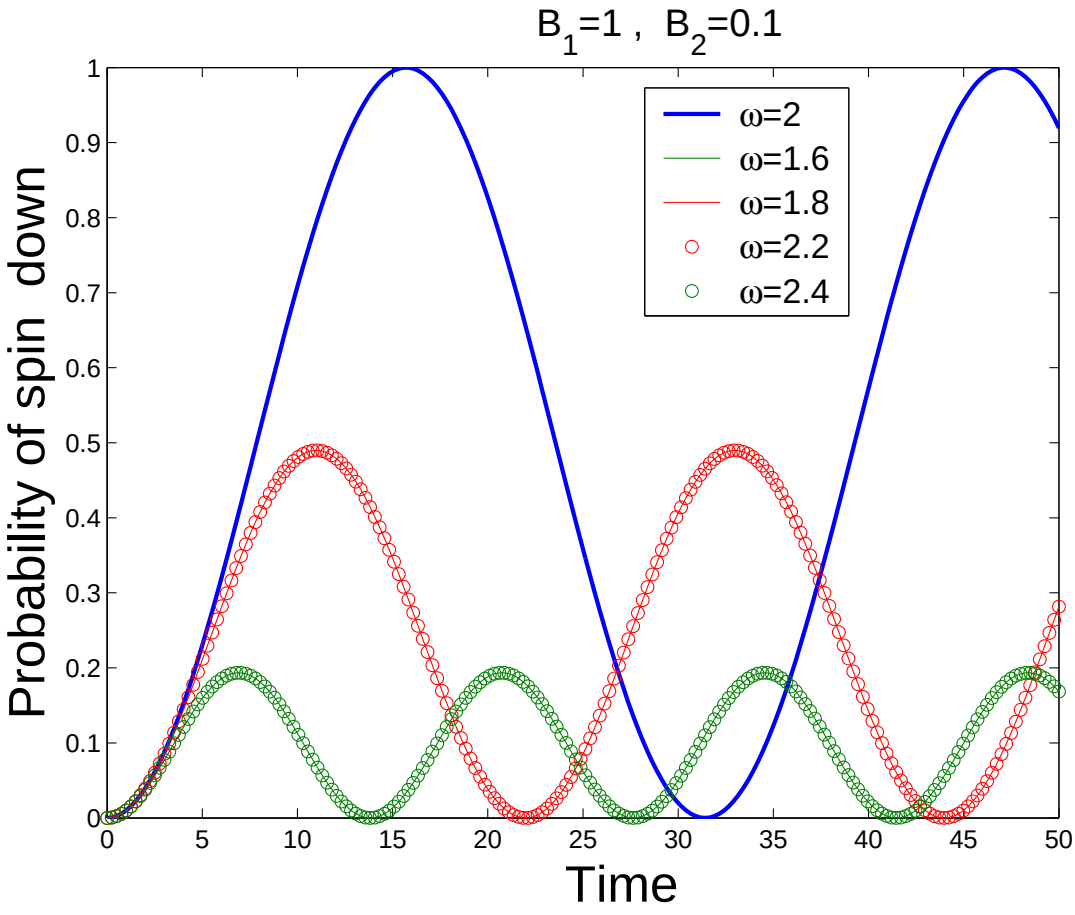

Figure A.1: When $\omega = 2$(unit of energy), the resonance occurs, i.e the max of probability of spin down is one. symmetrically, the max of probability of spin down decay with the fluctuation of the resonance frequency $\omega = 2$.

$$P_{\downarrow}(t) = \frac{B_2^2}{\left(B_1 - \frac{\omega}{2}\right)^2 + B_2^2} \sin^2\left(\sqrt{\left(B_1 - \frac{\omega}{2}\right)^2 + B_2^2}\, t\right) \tag{A.3}$$

The numerical result of Eq. (A.3) is shown in Fig. A.1. The strength of rotating field, B_2, is relative about the coupling between two states of spin up and spin down. In other word, The ability of spin flip resonance is proportional to the value of B_2. For example, the value of B_2 is more small, the full width at half maximum of resonance profile is shaper. It indicates that the frequency of $B_2(t)$ is necessary to closely match the Lamor frequency due to B_1 and then the resonance occurs.

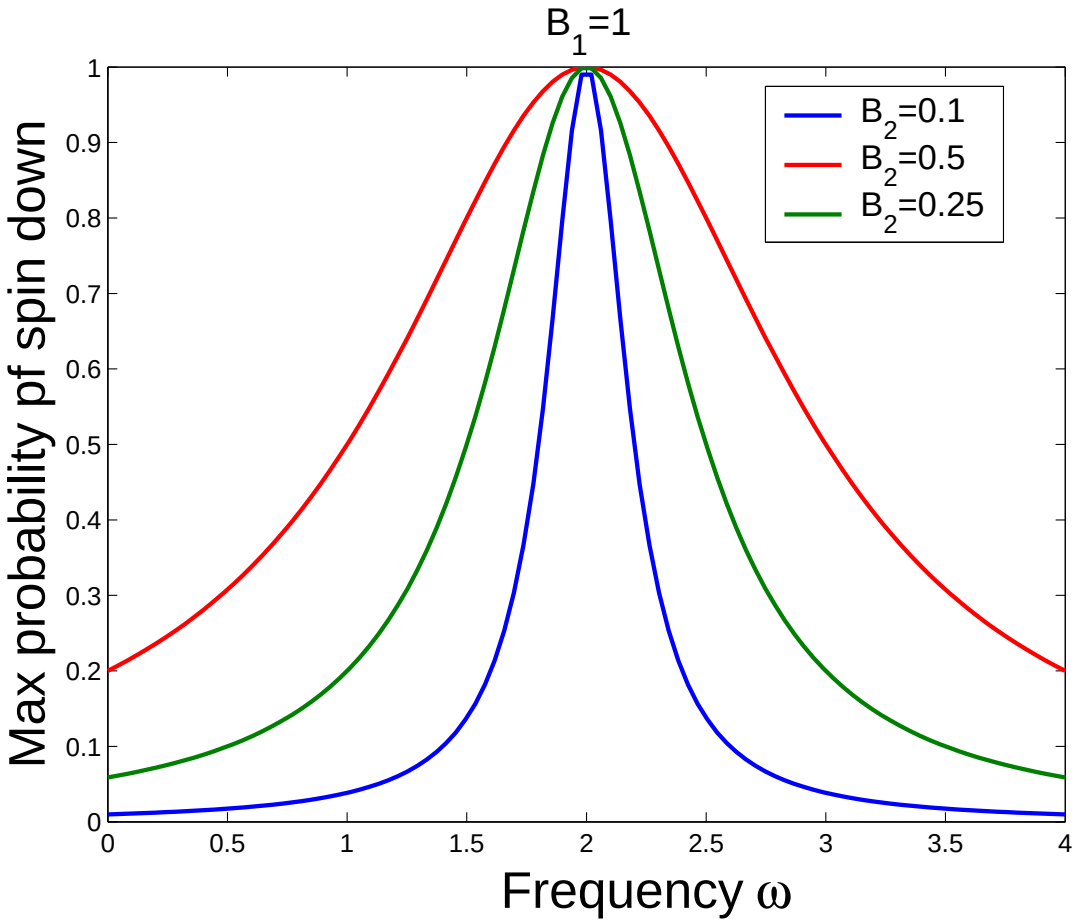

Figure A.2: The strength of rotating field, B_2, is proportional to the coupling between two states of spin up and spin down. The full width at half maximum of resonance profile is larger when the strength of rotating field, B_2, is larger.

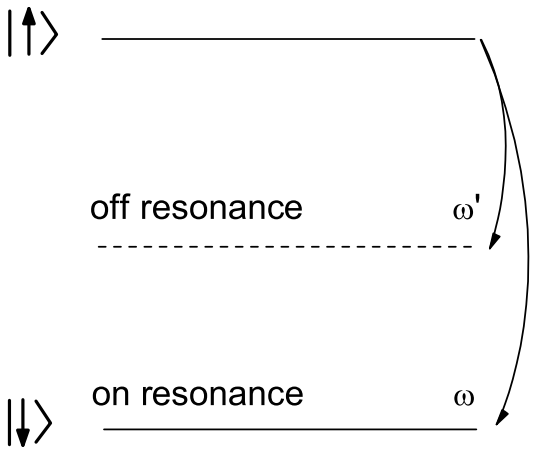

Figure A.3: The relation between NMR and sideband.

The relation between NMR and sideband is introduced in Fig. A.3. First, The sideband of rotating field B_2 offers a energy $\hbar\omega$ is not match with the energy difference between the two states of spin up and spin down. The spin flip happens but the probability is small, see in the Fig. A.1. On the other hand, the spin resonance occurs while the sideband match the state with large density of state. Second, although the sideband does not closely match the spin-down state the probability is enough large unless the coupling between the two spin states is strength enough, i.e. the value of B_2 is large enough, see Fig. A.2.

Appendix B

Derivation of particle current

We start the derivation from the Hamiltonian Eq. (B.1) which just is considered along longitudinal direction without subband mixing term $\frac{\alpha}{i}\frac{\partial}{\partial y}\sigma_x$

$$\left(-\frac{\partial^2}{\partial x^2}+i\alpha\frac{\partial}{\partial x}\sigma_y+b_0\sigma_x\right)\psi(x,t)=i\frac{\partial}{\partial t}\psi(x,t) \tag{B.1}$$

Producting $\psi^\dagger(x,t)$ on left hand side of Eq. (B.1), we can obtain

$$-\psi^\dagger(x,t)\left[\frac{\partial^2}{\partial x^2}\psi(x,t)\right]+i\alpha\psi^\dagger(x,t)\left[\frac{\partial}{\partial x}\sigma_y\psi(x,t)\right]+b_0\psi^\dagger(x,t)\left[\sigma_x\psi(x,t)\right]=i\psi^\dagger(x,t)\left[\frac{\partial}{\partial t}\psi(x,t)\right] \tag{B.2}$$

Taking dagger to Eq. (B.1) and product $-\psi(x,t)$ on right hand side of it, we can obtain

$$\left[\frac{\partial^2}{\partial x^2}\psi^\dagger(x,t)\right]\psi(x,t)+i\alpha\left[\frac{\partial}{\partial x}\psi^\dagger(x,t)\sigma_y\right]\psi(x,t)-b_0\left[\psi^\dagger(x,t)\sigma_x\psi(x,t)\right]=i\left[\frac{\partial}{\partial t}\psi^\dagger(x,t)\right]\psi(x,t) \tag{B.3}$$

The summation of Eq. (B.2) and Eq. (B.3) is

$$\begin{aligned}&\frac{\partial}{\partial t}\left[\psi^{\dagger}(x,t)\psi(x,t)\right]\\&=-\frac{\partial}{\partial x}\left[\psi^{\dagger}(x,t)\frac{1}{i}\frac{\partial}{\partial x}\psi(x,t)-\frac{1}{i}\frac{\partial}{\partial x}\psi^{\dagger}(x,t)\psi(x,t)-\alpha\psi^{\dagger}(x,t)\sigma_y\psi(x,t)\right]\end{aligned} \tag{B.4}$$

According to continuity equation,

$$\frac{\partial}{\partial t}\rho+\frac{\partial}{\partial x}J=0$$

the L.H.S. of Eq. (B.4) is regarded as time derivative of particle density and R.H.S of Eq. (B.4) is regarded as spatial derivative of particle current with respect to x. The compact format of particle current is shown as following

$$J(x,t)=\psi^{\dagger}(x,t)\left(-i\frac{\partial}{\partial x}-\frac{\alpha}{2}\sigma_y\right)\psi(x,t)+c.c. \tag{B.5}$$

where the abbreviation, c.c., is standing for complex conjugate of the former terms.

QED

Bibliography

[1] G. Dresselhaus, Phys. Rev. **100**, 580 (1955).

[2] E. I. Rashba, Fiz. Tverd. Tela (Leningrad) **2**, 1224 (1960) [Sov. Phys. Solid State **2**, 1109 (1960)]; Y. A. Bychkov and E. I. Rashba, J. Phys. C **17**, 6039 (1984).

[3] Mathias Duckheim and Daniel Loss, Nature Physics **2**, 195 (2006).

[4] *Chapet 4 in Landau Lavel Spectroscopy* , G. Landwehr and E.I. Rashba (Elsevier Science, 1991).

[5] Al. L. Efros and E. I. Rashba , Phys. Rev. B **73**, 165325 (2006).

[6] D.Sanchez, L.Serra and M. S. Choi, Phys. Rev. B **77**, 035315 (2008).

[7] J. Yao and Z. Q. Yang., Phys. Rev. B **73**, 033314 (2006).

[8] Zhongyao Li and Zhongqin Yang, Phys. Rev. B **76**, 033307 (2007).

[9] J.Nitta, T.Akazaki, and H.Takayanagi, Phys. Rev. Lett. **78**, 1335 (2006)

[10] T.P. Smith III and F.F. Fang, Phys. Rev. B. **35**, 7729 (1987)

[11] S. Pramanik and S. Bandyoppahyay, Phys. Rev. B **76**, 155325 (2007)

[12] C. S. Tang and C. S. Chu, Phys. Rev. B. **53**, 4838 (1996).

[13] L. Y. Wang, C. S. Tang, and C. S. Chu, Phys. Rev. B. **73**, 085304 (2006).

[14] *Page 555 ∼ 560 in Methods of theoretical physics part1*, P. Morse, H. Feshbach (McGraw-Hill College, June 1953).

[15] P. F. Bagwell and R. K. Lake, Phys. Rev. B. **46**, 15329 (1992).

[16] Y. Kato, R. C. Myers, A. C. Gossard, D. D. Awschalom, Nature Physics **427**, 50 (2004).